HIGH ENTROPY ALLOYS PROPERTIES AND ITS APPLICATIONS – AN OVERVIEW

S. John Mary[a], R. Nagalakshmi[b] and R. Epshiba[b,c]

Keywords: high entropy alloys, corrosion resistance, micro structure, properties, applications.

High entropy alloys are more corrosion resistance than 316L stainless steel HEA are used as implantation material Because its unique properties and better corrosion resistances behaviors. The improved corrosion behavior could be attributed to the different chemical composition as well as the formation of a unique high entropy atomic structure with a maximum degree of disorder. It is also possible to achieve high-hardness and high-abrasion performance at high temperature, microstructure and properties of several HEA. High entropy alloys are prepared by various methods such as powder metallurgy laser cladding etc, are discussed. The corrosion resistance of HEAs and its applications also discussed.

* Corresponding Authors
E-Mail: s_johnmary@yahoo.com

[a] Department of Chemistry, Loyola College, Chennai 600 034, India.
[b] Department of Chemistry, Aarupadai Veedu Institute of Technology, Chennai-603 104,
[c] Department of Chemistry, Sri Muthukumaran Institute of Technology, Chennai, India

Introduction

HEAs are loosely defined as solid solution alloys that contain more than five principal elements in equal or near equal atomic percent (at. %). The concept of high entropy introduces a new path of developing advanced materials with unique properties, which cannot be achieved by the conventional micro-alloying approach based on only one dominant element. Up to date, many HEAs with promising properties have been reported, e.g., high wear-resistant HEAs, $Co_{1.5}CrFeNi_{1.5}Ti$ and $Al_{0.2}Co_{1.5}CrFeNi_{1.5}Ti$ alloys; high-strength body-centered-cubic (BCC) AlCoCrFeNi HEAs at room temperature, and NbMoTaV HEA at elevated temperatures. Furthermore, the general corrosion resistance of the $Cu_{0.5}$NiAlCoCrFeSi HEA is much better than that of the conventional 304-stainless steel. In general, commercial alloy systems are based on one principal element and the total quantum of solute atoms is not large in many cases. In contrast, high-entropy alloys are equiatomic multi component alloys. These alloys form simple solid solutions due to the large configurational entropy. If these multi-metallic cocktails are made in nano crystalline state, they are expected to have high strength coupled with reasonable formability. Nanocrystalline high entropy alloys can be made easily by high energy ball milling.

Composition of High Entropy Alloys

High Entropy Alloys (HEA) are made of many metals mixed in desired Proportions. Usually the HEA's are made of Al, Fe, Co, Ni, Cr, Mg, Zn, K, and Cu. HEA's consisting of AlFeCoNiCr,[1] CaMgZn,[2] AlFeCoCrNiCu,[3] FeCoNiCrCu,[7,8] and FeCrNiAlLa.[14]

Methods of preparation of HEA's

High entropy alloys are made by several methods. They can be prepared in vacuum arc induction melting furnace,[1] equivalent thermal entropy method,[4] powder metallurgy method,[5] and simple casting method.[15]

Properties of High Entropy Alloys

High entropy alloys have unique properties and applications. Ca20Mg20Zn20Sr20Yb20 has biomedical application.[2] It promotes bone formation.

HEA's have high corrosion resistance. For example Al0.5FeCoCrNiCu has high corrosion resistance. Its resistance is better than that of 304 stainless steel in 0.5 mol L^{-1} H_2SO_4 solution and 1 mol L^{-1} NaCl solution.[3] Corrosion resistance of CrFeNiCuMoCo increases and its corrosion current density decreases.[5] AlCoCrFeNiTi0.5 alloy has good corrosion resistance in 3.5 % NaCl solution.[6] Tempering treatment of this alloy improves its corrosion resistance. Iron alloys have high strength and ductility. They have high resistance to oxidation and corrosion. They can be considered for structural metallic materials.[15]

The properties of high entropy alloys have been investigated by various techniques such as polarisation study[3,10,13] and AC impedance spectra.[16,19]

The surface morphology has been analyzed by methods such as SEM, EDS , X-rays diffraction,[5,8,17] selected area diffraction[14] and differential scanning colorimetry.[14] The surface of high entropy alloys has fcc phase and bcc phase.[1,3,13,14] Addition of one element to the *mixture* sometimes changes the phase. For examples when Al is added the phase of AlFeCoNiCrTi alloy changes from fcc to bcc phase.[13]

The composition of high entropy alloys, the methods of preparation of alloys, their properties, uses, methods of studying the HEA's, and the surface morphology of HEA's are summarised in Table 1.

Table 1. Preparation methods and properties of high entropy alloys

HEA	Preparation method/Properties	Method and Spectroscopy	Finding/Application	Ref
AlxFeCoNiCr(B)	High entropy alloys were prepared in a vacuum arc induction melting furnace.	Electrochemical investigation	The microstructure is a simple solid solution structure, and the fraction of FCC crystal structure decreased with increasing of Al content. Chromium tends to segregate at the inter-dendrite grain boundary	[1]
Ca65Mg15Zn20	A Ca20Mg20Zn20Sr20Yb20 high-entropy bulk metallic glass was fabricated with unique properties of high-entropy alloys.	In vitro tests, in vivo animal test	The mechanical properties and corrosion behavior were enhanced. The in vitro tests showed that the Ca20Mg20Zn20Sr20Yb20 high-entropy bulk metallic glass could stimulate the proliferation and differentiation of cultured osteoblasts. The in vivo animal tests showed that this high-entropy bulk metallic glass did not show any obvious degradation after 4 weeks of implantation, and they can promote osteogenesis and new bone formation after 2 weeks of implantation	[2]
AlxFeCoCrNiCu (x=0.25, 0.5, 1)	HEA is gradually changed from a single FCC to FCC phase and BCC phase with the addition of Al. With the addition of Al from *x*=0.25 to 1.0, the hardness of the alloys increase from 165 to 485 HV correspondingly	Polarization curves	The polarization curves show that alloys has the better corrosion resistance than 304 stainless steel in 0.5 mol L^{-1} H_2SO_4 solution and 1mol L^{-1} NaCl solution, and meanwhile Al0.5FeCoCrNiCu high-entropy alloy has the best comprehensive corrosion resistance.	[3]
K4169	The Cell Automatoin technology was adopted to coupled simulate the grain structure formation process of K4169 superalloy blade with its temperature fields using continuous nucleation model and kinetic model of dendrite tip growth	Equivalent thermal entropy method	In order to control the grain structure of K4169 superalloy blade which affects its mechanical performance and ability of resistance to corroding in high temperature state, the transient temperature field distributions were analyzed. The relationships between temperature and time of every point on vertical section and cross section during phase change heat transference process of K4169 superalloy were obtained.	[4]
CrFeNiCuMoCo	Powder metallurgy method	SEM/EDS, XRD micro-Vicker hardness test, electro-chemical methods	The morphology of the CrFeNiCuMoCo HEA is simple, the phase mainly composes of FCC and BCC; Mo and Cu are segregated in the alloy; the alloy shows excellent corrosion resistance, the corrosion current density decreases by an order of magnitude compared with 304 stainless steel	[5]
AlCoCrFeNiTi 0.5	The AlCoCrFeNiTi 0.5 high-entropy alloys fabricated by cold crucible levitation melting (CCLM)	Electrochemical methods	The alloy exhibits a superior resistance to tempering and softening property. The tempering treatment improves corrosion properties in a 3.5 % NaCl solution, and the alloy tempered at 700 °C exhibits the best corrosion property among the experimental alloys.	[6]

FeCoNiCrCu	Corrosion resistance of directionally solidified alloy is superior to that of the as-cast FeCoNiCrCu alloy	Potentiodynamic polarization	The results showed that only diffraction beak corresponding to a FCC crystal structure was observed in the directionally solidified FeCoNiCrCu alloy. With increasing solidification rate, the interface morphology would grows in planar, cellular and dendrite.	[7]
FeCoNiCrCu0.5	The as-cast and annealed alloys were severely corroded in 3.5 % NaCl solution with precipitation of the Cu-rich phase in the matrix. The potential of this phase differed considerably from that of the matrix. The Cl^- ions preferentially attacked this susceptible area.	X-ray diffraction, SEM, TEM.	This study examined the microstructure and electrochemical corrosion behaviour of high-entropy FeCoNiCrCu0.5 alloys annealed at various temperatures.	[8]
FeCoNiCrCu	The alloy was prepared by arc melting technique, when the coating is amde without Si, Mn and Mo additions, the microstructure is mainly composed of columnar and equiaxed grains with uni-formly distributed alloying elements	Arc melting, laser cladding	The influences of Si (1.2 mol %), Mn (1.2 mol %) and Mo (2.8 mol.%) additions on the microstructure, properties and coating quality of laser cladded FeCoNiCrCu high-entropy alloy coating have been investigated.	[9]
Co1.5CrFeNi1.5Ti0.5Mox	The corrosion resistance of the Mo-free alloy was superior to that of the Mo-containing alloy	Potentiodyna-mic polarisa-tion	Electrochemical properties of the Co1.5CrFeNi1.5Ti0.5Mox high-entropy alloys in three aqueous environments which simulate acidic, marine, and basic environments at ambient temperature (~25°C) were studied.	[10]
AlFeCoNiCrTiVx	The alloy system had better corrosion resistance than 304 stainless steel in 0.5 mol L^{-1} H_2SO_4 solution and 1 mol L^{-1} NaCl solution, and the AlFeCoNiCrTiV 0.5 alloy had the best comprehensive corrosion resistance.	Polarization curves	The microstructure and electrochemical properties of equiatomic and high entropy AlFeCoNiCrTiV x, (x, molar ratio, x=0.5, 1, 1.5, 2) alloys were investigated in 0. 5 mol L^{-1} H_2SO_4) solution and 1 mol L^{-1} NaCl solution, and compared with 304 stainless steel.	[11]
Bulk and thin film intermetallic alloys	Connected with the entropy gain, the degree of order depends on temperature and thereby the stability of the designed beneficial materi-als properties is affected. By monitoring changes in the degree of atomic order an access to atom migration is gained, which is comple-mentary to the usual diffu-sion experiments, where the degree of order is not chan-ged on average.	Thermal treatment	Due to their excellent corrosion resistanceand their advantageous mecha-nical and in many cases also magnetic properties, intermetallic alloys are among the most important materials of the 21st century. Most of their outstanding qualities are linked to long-range order, the fact that unlike atoms are preferred as neighbours, which then segregate to different sublattices.	[12]

AlxFeCoNiCrTi	By using of the strategy of equiatomic ratio and high entropy of mixing. The composition of the alloy system is gradually changed from FCC phase and BCC phase to a single BCC phase with the addition of Al.	Polarization curves	The alloy has better corrosion resistance than 304 stainless steel and AlFeCuCoNiCrTix high-entropy alloys in 0.5 M H_2SO_4 and 1 M NaCl solutions, and that the AlFeCoNiCrTi alloy has the best comprehensive corrosion resistance.	[13]
FeCrNiAlLa alloy, with high (> 40 %) chromium content.	Surface layer (≤1 μm thickness) of the mechanically polished specimen of the alloy Fe44Cr1Ni4Al0.3La consists of the amorphous Beilby layer and that its adjacent matrix layer, crushed due to the plastic deformation, formed an entropy "excited" functional system, which at the temperature of 1200 °C in laboratory atmosphere permits the formation of an oxide surface layer with a micro-wrinkles modulated structure of uniform thickness, in the form of mixture of nanocrystallites (100 ÷500nm) made of oxides of atoms constituting the basic metallic matrix. Beneath this layer a thin alumina scale is observed to form. Increasing the oxidation temperature causes the regrowth of nanocrystallites and also the recrystallization processes, accompanied by solid-phase reactions between oxide nanoparticles.	SEM, Auger electron spectrometry fast electron diffraction (FED) in the "on reflection" regime and wavelength dispersive spectrometry	The Al_2O_3 layer is characterized by high adherence with metallic substrate and provides protective features against both high temperature (1200 °C) oxidation of the matrix and resistance to abrasion. By the pretreatment at 1200 °C of the investigated alloy's surface modified specimens, there forms a low thickness (several microns) scale which has ultra fine graininess (∼1 μ) with no porosity and blocked grain boundaries short-circuit diffusion paths. This gives to the scale the ability to protect the metallic matrix against high temperature gas (and other aggressive environment) corrosion.	[14]
Based (Fe) alloy	The iron alloy was prepared by a simple casting method, to obtain a hierarchical structure, with better mechanical performance. The alloy was composed of milli-scale lathy, micro-scale denritic phases, nanoscale crystalline particles, and a glassy matrix, with short-range order of a length scale less than 1 nm.	Simple casting method	It was observed that the alloy showed significant highstrength and ductility, high resistance to oxidation and corrosion that were superior in comparison to most of the high-strength iron alloys. It was also found that these properties of the alloy made it a potential candidate, to emerge as a structural material that may serve as a design consideration for the development of structural metallic materials.	[16]

Al0.5CoCrCuFeNiBx alloys	High entropy alloys are a newly developed family of multi component alloys that consist of various major alloying elements, including copper, nickel, aluminum, cobalt, chromium, iron, and others. Each element in the alloy system is present at between 5 and 35 atom %.	Anodic polarization curves electrochemical impedance spectra	This investigation discusses the corrosion resistance of the Al0.5 CoCrCuFeNiBx alloys with various amounts of added boron. Surface morphological and chemical analyses verified that the addition of boron produced Cr, Fe, and Co borides. Therefore, the fraction of Cr outside borides precipitates was scant.	[16]
High entropy alloys	(HEAs) are a newly developed family of multi-component glassy alloys composed of several major alloying elements, such as copper, nickel, aluminum, cobalt, chromium, iron, silicon, titanium, etc.. The dendritic phase was composed mainly of a non-crystalline phase with a little body centered cubic (BCC) structure whereas the interdendritic phase had an amorphous structure containing small amounts of nano-scale precipitates.	XRD, selected area diffraction (SAD), and DSC analysis, Anodic polarization curves	Tests in 1 N sulfuric acid containing different concentrations of chloride ions showed that the HEA has least resistance to general corrosion at a chloride ion concentration of 0.5 M (close to the concentration in seawater). The lack of hysteresis in cyclic polarization tests confirmed that the HEA-like 304S-is not susceptible to pitting corrosion in chloride-free 1 N H_2SO_4.	[17]
MB-50 alloy	The high corrosion resistance of the alloy, caused by very low solubility of its components in mercury is demonstrated.	Thermal cycling	Corrosion resistance of an MB-50 alloy in mercury is studied at 473 and 573 K under conditions of thermal cycling.	[18]

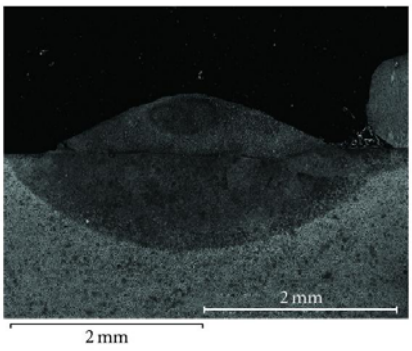

Figure 1. Macroscopic images of SEM of AlxFeNiCuCr high entrophy alloys

Conclusion

High entropy alloys (HEAs), (equiatomic multicomponent alloy) are in a single solid –solution form. They have unique mechanical and corrosion resistances properties. Hence they are used as implantation materials. They have fcc or bcc structure. These structures are inter convertible on addition of some foreign substances. The microstructure, hardness, corrosion resistance and compression resistance have made these HEAs unique. They can be prepared by various methods such as powder metallurgy and laser cladding. Their microstructures have been investigated by SEM, TEM and RD. Corrosion resistance has been evaluated by polarization study and Electrochemical Impedance spectra.

Acknowledgement

The authors are thankful to their management for their help and encouragement.

REFERENCES

[1]Liu, C.-G., *J. Alloys Comp*d., **2013***, 553*, 216.

[2]Li, H. F., Xie, X. H., Zhao, K., Wang, Y. B., Zheng, Y. F., Wang, W. H., *Acta Biomaterialia,* **2013***, 9(10)*, 8561-8573

[3]Niu, X.-L., Wang, L.-J., Sun, D., Julius, J., *J Funct. Mat*er., **2013***, 44(4).* 532

[4]Liu, H., Ren, H., Dong, D., *Appl Mech Mat*., **2012** *,217-219.* 330.

[5]Qiu, X.-W., Zhang, Y.-P., *Mater. Sci. Eng. Powder Metall*., **2012,** *17(3),* 377 .

[6]*Yu, Y., Xie, F., Zhang, T., Kou, H.,Hu, R., Li, J. Rare Metal Mat Eng*., **2012**, 41 (5) , 862.

[7]Cui, H., Zheng, L., Wang, J., *Appl. Mech. Mater*., **2011***, 66-68*, 146.

[8]Lin, C.-M., Tsai, H.-L., *Mater. Chem. Phys*., **2011***, 128(1-2),* 50.

[9]Zhang, H., Pan, Y., He, Y.-Z., *Mater. Design*., **2011***, 32(4),* 1910.

[10]Chou, Y.L., Yeh, J.W., Shih, H.C., *Corros. Sci.,* **2010***. 52(8),* 257.

[11]Luo, X.-Y., Liu, G.-Z., Li, W., Guo, J.-J., *Corros. Protect.,* **2010,** *31(5),* 355.

[12]Pfeiler, W., Puschl, W., Issro, Ch., Kozubski, R., Pierron-Bohnes, V., *Mater. Res. Soc. Symp. Proc*.., **2009**, *112*, 507.

[13]Li, W., Liu, G.-Z., Guo, J.-J., *Zhuzao/Foundry*, **2009,** *58(5*), 431.

[14]Tsurtsumia, O., Kutelia, E., Bulia, B., Mikadze, O., *Mater. Sci. Forum*., **2008***, 595-598*, *PART 2,* 833.

[15]Wang, J.-G., Zhao, D.-Q., Pan, M.-X., Wang, W.-H., *Adv. Eng. Mater*., **2008***, 10(1-2), 46.*

[16]Lee, C. P., Chen, Y. Y., Hsu, C. Y., Yeh, J. W., Shih, H. C., *J. Electrochem. Soc.,* **2007***, 154(8), C4, 2008 24-C430.*

[17]Chen, Y. Y., Duval, T., Hung, U. D., Yeh, J. W., Shih, H. C., *Corros. Sci*., **2005**, 47(9), 2257.

[18]Kozbagarova, G. A., Musina, A. S., Mikhaleva, V. A. Kozbagarova, G. A., Musina, A. S., Mikhaleva, V. A., *Prot. Met.,* **2003***, 39(4*), 374.

[19]Zarrok, H., Zarrouk, A., Salghi, R., Ebn Touhami, M., Oudda, H., Hammouti, B., Touir, R., Al-Deyab, S. S., *Int. J. Electrochem. Sci*., **2013,** *8(4)*, 6014.

„

Received: 12.03.2015.
Accepted: 05.07.2015.

DETERMINATION OF CANCER ANTIGEN CA15-3 AND ALPHA FETO PROTEIN (AFP) LEVELS AS TUMOR MARKER IN PATIENTS WITH BREAST AND PROSTATE CANCER

Rana Kareem Al- Saady[a] and Salah Mohammed Fizea[a]*

Keywords: CA15-3, AFP, breast cancer, prostate cancer.

The objective of the present study is to evaluate the values of cancer antigen (CA15-3) and alpha feto protein (AFP) in patients with breast and prostate cancer. The results revealed the values for CA 15-3 in serum of G1 showed a highly significant increase compared to normal healthy subjects, but CA15-3 in serum of G2 was compatible with control. The results showed the value of serum AFP in G1 (was not significant different) when compared to control, while a highly significant difference in G2 was noticed when compared to healthy subjects.

*Corresponding Authors
E-Mail: salahmf79@yahoo.com
[a] Department of Chemistry, College of Education for Pure Science, Ibn Al-Haitham, University of Baghdad

Introduction

Tumor markers are biochemical substances elaborated by tumor cells either due to the cause or effect of malignant process. A tumor marker produced by the tumor and, when present in significant amounts, indicates the presence of a cancer.[1, 2]

Cancer antigen CA15-3 is heterogeneous 300 KD glycoprotein antigen was defined by using two monoclonal antibodies 115D8 and DF3 raised against breast carcinoma cells. The diagnostic sensitivity of the CA15-3 for breast carcinoma is low as its elevated levels are also observed in benign breast diseases and in liver cirrhosis, acute and chronic hepatitis. The marker concentration is also elevated in metastatic cancers of pancreas, ovary, colorectal, lung, stomach, and uterus.[3,4]

Alpha feto protein (AFP), a very popular and extensively studied carcino embryonic glycoprotein/oncofetal antigen, is a major fetal serum globulin with a molecular weight of approximately 65,000 D. The single chain glycoprotein has carbohydrate content of 3 % and amino acid sequence similar to that of albumin. It is expressed either during malignancy or during intra uterine or early postnatal life.[5,6] An increase in serum AFP concentration below 400 ng mL^{-1} was also reported in 10-15 % of cases of acute and chronic hepatitis, liver cirrhosis and secondary hepatic malignancies.[7,8]

Experimental part

The study was carried out on 71 subjects comprising of 36 patients with breast cancer G1, 10 patients with prostate cancer G2, and 25 normal healthy controls with range of (40-55) years. The patients were admitted to Al Khadmiya Teaching Hospital for treatment.

Blood sample 3 mL were collected left at room temperature for 15 min centrifuged at (3000 rpm). Serum was separated and freezed until time of analysis.

Serum CA 15-3 determination

Serum CA15-3 was estimated using a kit (DrG, Germany), the analysis based on the principle of a solid phase enzyme linked immunosorbent assay (ELISA).[9,10] The concentration of CA15-3 was evaluated from standard curve drawn between standards of CA15-3 provided with the kit and absorbance at 450 nm.

Serum AFP determination

Serum AFP was estimated using a kit (BioCheck, USA), the analysis based on the principle of a solid phase enzyme linked immunosorbent assay (ELISA)[11]. the concentration of AFP was evaluated from standard curve drawn between standards of AFP provided with the kit and absorbance at 450 nm.

Statistical Analysis

The results were expressed as mean±SD of mean, using Statistical Package for Social Sciences (SPSS) version 19.0 and Microsoft Excel 2010 for data processing and graph construction. Statistical significant difference was ($p \leq 0.05$) .and highly significant difference was ($p \leq 0.001$).

Results and Discussion

The values of serum CA15-3 and AFP of breast cancer G1 , prostate cancer G2 and healthy subjects G3 are shown in Table 1.

Table 1. Value mean±SD for CA15-3 and AFP in all studied groups.

Group	CA15-3 U mL^{-1}	*P*	AFP ng mL^{-1}	*P*
Control *N*=25	18.18 ±4.42		3.98±1.20	
G1 *N*=36	52.65 ±10.37	≤0.001	4.59±1.05	>0.05
G2 *N*=10	20.25 ±1.68	>0.05	8.43±0.59	≤0.001

CA 15-3 in serum of G1 showed a significant increase compared to normal healthy subjects, but CA15-3 in serum of G2 was compatible with control.

Recent study suggest that a very slight increase in CA15-3 of breast cancer in few patients indicating a chance of disease progression or recurrence.[12] CA15-3 serum levels are influenced by disease extent.[13] Another study also reported an elevated level of CA 15-3 in metastatic condition.[14] Elevated CA15-3 levels are more common in metastatic breast cancer patients than with other tumor markers.[15]

The role of tumor markers in the management of breast cancer patients is limited to patients with advanced disease, This is because that they are rare abnormal in early disease or with local recurrence. Thus tumor marker analysis is appropriate in previously diagnosed patients at high risk for recurrence to detect early disease dissemination and in patients with metastatic disease to evaluate therapeutic response.[14]

A recent study suggested that serum tumor markers are abnormally elevated in patients with breast cancer. CA15-3 is useful clinical marker, good indicator of disease extent and may have important prognostic value. One of the main request for an ideal cancer marker it is suitability for preclinical screening. Therefore, prerequisite would be high sensitivity as well as specificity with respect to the detection of primary breast cancer.[16] Other study showed CA 15-3 to be one of the first circulating prognostic factors for breast cancer. Preoperative concentration thus might be combined with existing prognostic factors for predicting out come in patients with newly diagnosed breast cancer .and thus CA15-3 is the most widely used serum marker in breast cancer,[17] also other study suggested that circulating CA15-3 antigen level are elevated in more than 70 % of breast cancer patients with distant metastases.[18] CA15-3 has been found useful in monitoring the course of advanced breast cancer and in the postsurgical follow-up of patients with breast carcinoma.[19] CA- reactive antibodies 115D8 and Df3 detect individual antigen that are present in human primary epithelial carcinoma.[20] Ninety-three percent of 140 human epithelial primary tumors reacted with monoclonal antibodies 115D8 or Df3, including breast, ovarian, lung, and also colon and gastric carcinoma.[21] In general, changes in tumor markers accurately and consistently reflected changes in disease status but not in the pertinent issue, However the use of tumor markers in clinical practice will lead to more effective treatment remain controversial.CA15-3 is a marker of distant metastasis in breast carcinoma with high specificity and moderate sensitivity.[22]

From the same table the value of serum AFP in G1 showed no significant difference when compared to control , while a highly significant difference in G2 when compared to healthy subjects was noticed.

Recent study demonstrated that AFP together with other serum markers is a well known useful clinical tool for diagnosis and follow up of patients with germ cell tumors. However many different benign and malignant clinical condition may represent serum elevation of AFP without germ cell tumor growth. Therefore all clinical conditions characterized by serum AFP increase, other than germ cell tumor, have to be taken into account before assuming that the elevation of AFP reflects the activity of this malignancy.[23] Other tumors have been associated with elevated AFP plasma levels such as pancreatic cancer (23 %), gastric cancer (20 %), bronchial cancer (7 %), colorectal cancer (5 %), and with lower frequency in cancer of the esophagus, small bowel, gallbladder, breast, endometrium, kidney, prostate and metastatic liver disease.[24]

Conclusion

A conclusion could be drawn from this study that CA15-3 elevated in breast cancer cases only, while AFP elevated in prostate cancer cases only.

References

[1]Del Villano, B. C., Brennan, S., Brock, P., *Clin. Hem*., **1983**, *29*, 549-52.

[2]Bhattacharya, S., Siegel, E. R., Petersen, G. M., Chari, S. T., Suva, L., Haun, R. S., *Neoplasia*, **2004**, *6*, 674-86.

[3]Helfrich, G., Klapdor, U., Bahlo, M., In: Klapdor, R (ed.): New tumor markers and their monoclonal antibodies – actual relevance for diagnosis and therapy of solid tumors. *4th Symp. Tumor Markers*, Hamburg **1986**, George Thieme Verlag, Stuttgart New York, **1987**, 287-90.

[4]Aabo, K., Pedersen, H., Kjaer, M., *Eur. J. Cancer Clin. Oncol.,* **1986**, *22,* 211-7.

[5]Wu, J. T., Knight, J. A., Knight, D. P., CEA in the clinical diagnosis and treatment of colorectal cancer. In: ACP Clinical Chemistry Check Sample, *III. Am. Soc. Clin. Pathol*., Chicago, 1986.

[6]Malati, T., Saraswathi, A., Vittal, P. V., Ananth Reddi, P., *Asian J. Clin. Sci*., **1988**, *8*, 33-5.

[7]Malati, T., *Clin. Proc. NIMS*, **1989**, *4*, 169-74.

[8]Wang, P. Y., *Chung-Hua Chun Liu Tsa Chih*, **1991**, *13*, 61-3.

[9]Morimoto, H., Tanigawa, N., Inoue, H., *Cancer*, **1988**, *61*, 84-8.

[10]Chittoor, S., Swain, S., *Am. Fam. Physic.*, **1991**, *44,* 453-462.

[11]Engall, E., *Methods in Enzymology*, Van Vunakis, H., and Langone, J. J.(eds), Academic Press, NewYork, **1980**, *70*, 419-492.

[12]Prabasheela, B. and Arivazhagan, R., *Int. J. Pharm. Bio Sci*., **2011**, *2(2)*, 34-38.

[13]Tampellini, M., Gorzegno, G., Sarobba, G. M., Durando, A., Arese, P., Manzen, E., Castiglione, F., Malters, A., De, Nuzzo, F., Dogliottti, L., *Eur. J. Cancer*, **1998**, *34(5)*, 105.

[14]Ann Dnistrian, A., Morton Schwartz, K., Ernest Greenbery, J., Carol Smith, A., and Delia Schwarty, C., *Clin. Chim. Acta,* **1991**, *200*, 81 – 94.

[15]James, T. W. U., In: Henry JB (eds). *Clinical Diagnosis and Management by Laboratory Methods,* 20th Edn, New York, WB Saunders, **2001**, 1028 - 1042.

[16]Verring, A., Clouth, A., Ziolkowski, P., and G. Oremek, M., *J Isr . Pathol.*, **2011**.

[17]Michael, J., Duffy, J., *Clin. Chem*., **2006**, *52(2)*, 345-351.

[18]Colomer, R., Ruibal, A., Genollk, J., & Salvador, L., *Brit. J. Cancer*, **1989**, *59*, 283-286.

[19]Hayes, D. F., Zurawski, R., Kufi, W., *J. Clin. Oncol.*, **1986,** *4*, 1542.

[20]Hilkens, J., Buijs, F., Hilgers, J., *Int. J. Cancer*, **1984**, *4*, 197.

[21]Zotter, S., Hageman, P. C., Mool, J. W., Lossnitzer, A. and Hilger, J., *Cancer Res*., **1989.**

[22]Tomlinson, I. P. M., Whyman, A., Barrett, J. A., and Kremer, J. K., Eur. J. Cancer, **1995**, *3H(6),* 899-902.

[23]Iafrate, M., Rossato, M., *J. Androl. Sci.*, **2009**, *16,* 21-24.

[24]Schefer, H., Mattmann, S., Joss, R. A., *Ann Oncol*., **1998**, *9*, 667-72.

Received: 14.05.2015.
Accepted: 07.07.2015.

WEAK INTERMOLECULAR INTERACTION AND LATTICE ENERGY ANALYSIS OF SOME BENZOTHIAZOLE DERIVATIVES

Ratika Sharma[a] and Rajni Kant[a]*

Keywords: crystallography, benzothiazole, lattice energy, intermolecular interactions, hydrogen bonding.

A series of four chemically-similar-looking benzothiazole structures have been analyzed for their crystallographic comparison, weak intermolecular interaction analysis and lattice energy calculations. All the crystal structures are planar. However, the hydrazinyl group is slightly deviated with respect to the benzothiazole moiety in each structure. The N-H...N hydrogen bond plays an important role in the stabilization of the crystal packing in these derivatives. The related interactions of the type N-H...π, C-H...S and N....N act as an important linkage in most of the molecular pairs. A computational method has been used for the quantification of intermolecular interactions, as it allows partitioning of total interaction energy into corresponding coulombic, polarization, dispersion and repulsion contribution which facilitates a better understanding of the nature of intermolecular interactions contributing towards the crystal packing. The dispersive energy, however, lends significant contribution to the stabilization of these structures, thus making the combined nature of interaction energy in all the four molecules as predominately dispersive.

*Corresponding Author
[a] X-ray Crystallography Laboratory, Department of Physics and Electronics, University of Jammu, Jammu Tawi - 180006, India.
Tel/Fax [O]: +91 191 243 2051
E-Mail: rkant.ju@gmail.com

Introduction

Benzothiazoles, a class of sulfur and nitrogen containing heterocyclic compounds, have received considerable attention in recent years because of their medicinal and pesticidal importance. They possess considerable activity, including potent inhibition of human immune deficiency virus type 1 (HIV-1) replication by HIV-1 protease inhibition,[1] antitumor,[2] anthelmintic,[3] analgesic and anti-inflammatory,[4] antimalarial,[5] antifungal, anticandidal activities[6] and various activities related to the central nervous system.[7] As a part of our ongoing research work on the preparation of X-ray diffraction quality single crystals and their X-ray structure analysis, we have taken up four chemically-similar-looking compounds for their comparative crystallographic analysis, weak interaction analysis and the energy contributions. The Crystallographic Information File (CIF) for each compound was obtained through the licensed CSD access. All important molecular motifs which provide maximum stabilization to the crystal structure were extracted and the nature and energy of these pairs was determined using PIXEL[8].

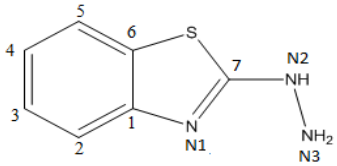

Figure 1. Chemical structure of benzothiazole moiety with atom numbering schemes

Structural features of benzothiazole structures

A representative view of benzothiazole moiety indicating the atomic numbering scheme is shown in Fig.1. The chemical name, molecular code and chemical structure for each compound is presented in Table 1.

Table 1. Chemical name, coding scheme and chemical Structure of the compounds

Chemical Name	Code	Chemical Structure
2-Hydrazinyl-benzo[d]thiazole[9]	M-I	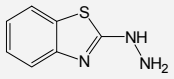
6-Chloro-5-fluoro-2-hydrazinyl benzo[d]thiazole[10]	M-II	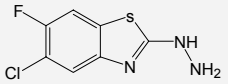
2-Hydrazinylmethyl-benzo[d]thiazole[11]	M-III	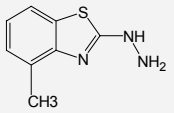
5-Chloro-2-hydrazinyl-benzo[d]thiazole[12]	M-IV	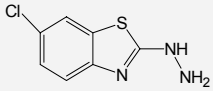

The precise crystallographic data for each compound is presented in Table 2. Most of the geometrical parameters, i.e., bond lengths and bond angles are in agreement with the literature values[13-15]. Some important bond lengths, bond angles and torsion angles are presented in the Table 3. All the crystal structures are planar, except the hydrazinyl group which is slightly deviated with respect to the benzothiazole moiety.

Table 2. Precise crystallographic data of four benzothiazole derivatives

Data	M-I	M-II	M-III	M-IV
Formula	$C_7H_7N_3S$	$C_7H_5ClFN_3S$	$C_8H_9N_3S$	$C_7H_6ClN_3S$
No. of molecules per unit cell, Z	4	4	2	8
Crystal System	Monoclinic	Monoclinic	Monoclinic	Orthorhombic
Space group	$P2_1/n$	$P2_1/c$	$P2_1$	$Pca2_1$
Cell parameters:				
a, Å	10.839(5)	11.129(6)	3.893(2)	13.023(13)
b, Å	507552(5)	5.664(3)	7.312(4)	5.770(6)
c, Å	12.961(5)	13.342(7)	14.137(8)	21.708(2)
α, ◦	90.00(5),	90.00	90.00	90.00
β, ◦	110.00(5)	108.55	93.42(1)	90.00
γ, ◦	90.00(5)	90.00	90.00	90.00
R-factor	0.037	0.024	0.028	0.019

Table 3. Selected bond lengths, angles and torsion angles

S. No.	Bond Length	M-I(Å)	M-II (Å)	M-III (Å)	M-IV (Å)		Average(Å)
					A	B	
1	N1-C7	1.305(3)	1.3109(11)	1.289(2)	1.3129(13)	1.3137(13)	1.3069
2	N2-C7	1.341(3)	1.3483(11)	1.375(3)	1.3743(10)	1.3437(10)	1.3510
3	N2-N3	1.413(3)	1.4172(10)	1.420(2)	1.4154(10)	1.4173(10)	1.4165
4	S1-C7	1.759(3)	1.7625(10)	1.756(2)	1.7639(10)	1.7621(10)	1.7612
5	S1-C6	1.748(2)	1.7429(9)	1.746(2)	1.7471(10)	1.7445(10)	1.7457
6	C3-C2	1.380(3)	1.3910(13)	1.389(3)	1.3877(15)	1.3935(14)	1.3882
7	C3-C4	1.385(4)	1.3977(13)	1.379(3)	1.4002(15)	1.3946(15)	1.3913
8	C4-C5	1.381(3)	1.3839(12)	1.387(3)	1.3921(15)	1.3934(15)	1.3723

S. No.	Bond angle	M-I(◦)	M-II (◦)	M-III (◦)	M-IV (◦)		Average (◦)
					A	B	
1	C6-S1-C7	88.2(1)	88.2(4)	87.97(10)	88.28(5)	88.34(5)	88.19
2	C7-N2-N3	117.7(2)	117.01(8)	115.08(15)	117.22(8)	117.51(8)	116.90
3	N1-C7-N2	123.1(2)	122.9(9)	123.57(18)	123.12(9)	123.24(9)	123.18
4	N1-C7-S1	120.5(2)	116.9(9)	117.74(15)	116.75(8)	116.56(8)	117.69
5	C1-N1-C7	110.2(2)	109.48(8)	109.43(16)	109.67(9)	109.88(8)	109.73

S. No.	Torsion Angles	M-I(◦)	M-II(◦)	M-III(◦)	M-IV(◦)	
					A	B
1	N3-N2-C7-S1	168.26	11.09	17.42	-9.96	-7.43
2	N3-N2-C7-N1	-12.10	-169.63	-165.98	170.89	172.50
3	N1-C1-C6-C5	-0.13	-177.75	-179.26	178.70	178.90
4	C2-C1-C6-S1	-0.28	177.75	179.72	-178.92	-178.94

The torsion around N2-C7 bond is insignificant. The hydrazinyl group located at the thiazole moiety is oriented in a *synperiplanar* (*cis*) or *antiperiplanar* (*trans*) conformation. In order to throw some more light on the molecular structure of benzothiazole derivatives, especially with regard to the role of hydrogen bonding, and the lattice energy calculations, the present work has been contemplated.

Hydrogen bonding analysis

Hydrogen bonding plays a key role in molecular recognition and crystal engineering. For this reason, crystal-packing studies are essential to understand the laws governing the intra- and inter-molecular H-bonding in a molecular crystal.

Table 4. Geometry of intermolecular hydrogen bonding in M-I – M-IV

Molecule	D-H…A	D-H, Å	H…A, Å	D…A, Å	θ[D-H…A, ◦]
M-I	N-H…N	0.90	2.04	2.93	175.0
	N-H…N	0.82	2.54	3.23	144.0
	N-H…N	2.44	2.54	3.34	167.0
M-II	N-H…N	0.89	2.30	2.99	135.0
	N-H…N	0.92	2.21	3.07	156.0
M-III	N-H…N	0.81	2.13	2.94	176.9
	N-H…N	0.85	2.44	3.13	
					139.5
M-IV	N-H…N	0.89	2.03	2.90	170.5
	N-H…N	0.89	2.05	2.95	175.3
	N-H…N	0.83	2.53	3.17	135.6

The usual convention for the representation of the hydrogen bond is **D-H…A,** where D is the donor and A is the acceptor.

In hydrogen bonds, the distance between the hydrogen and the acceptor atom is shorter than the sum of their van der Waals radii[16]. Weak hydrogen interactions like C-H...π and ***π–π*** have been recognized to play an important role in crystal structures of small biological molecules and protein structures[17-19].

Table 5. Hydrogen bonding data

Properties	Very strong	Strong	Weak	Molecule. I-IV
D…A range, Å	2.2-2.5	2.5-3.2	3.0-4.0	2.90-3.34
H…A range, Å	1.2-1.5	1.5-2.2	2.0-3.0	2.04-2.54
θ(D-H…A) range, (◦)	175-180	130-180	90-180	135-176
Effect on crystal packing	Strong	Distinctive	Variable	Variable

All the crystal structures are stabilized by N-H...N hydrogen bonding except for the molecule I which includes weak N-H...π interactions as well. The geometry of intra- and intermolecular hydrogen bonds is presented in Table 4. All the interaction parameters [H...A, D...A and θ] have been compared with the literature values[18] [Table 5] and following observations have been made:

The average values of H...N distance in molecule I-IV are 2.29, 2.26, 2.28 and 2.20 Å, respectively. Thus making these interactions fall under the category of strong to weak interactions with over all range comes out to be (2.04-2.54). A weak N-H...π interaction has also been identified in molecule-I that plays a crucial role in the stabilization of its crystal structure.

The average values of N-H...N distance in molecules I- IV are 3.09, 3.03, 4.51, 3.01 Å, respectively, thereby making such interactions fall under the category of strong to weak interactions. The angular range [θ(D-H...A)] of 135º -176º also supports this observation.

Energy calculations and discussion

In order to dwell more on the role of hydrogen bonding in small molecular assemblies of this kind, we have computed lattice energies of all the compounds by using the Coulomb-London-Pauli (CLP) model of intermolecular coulombic, polarization, dispersion and repulsion energies[20], known as the PIXEL method. Two output files are generated after the end of the calculation. The first (.pri file) consists of the total lattice energies partitioned into their coulombic, polarization, dispersion and repulsion contributions (Table 6). The second (mlc file) consists of molecule–molecule interaction energy along with the symmetry elements which relate to the molecules.

Table 6. Lattice energy from CLP (in kJ mol^{-1})

Molecule	E_{Coul}	E_{Pol}	E_{Disp}	E_{Rep}	E_{Tot}
M-I	-90.6	-41.9	-124.0	127.0	-128.9
M-II	-96.9	-41.9	-152.8	155.4	-143.2
M-III	8.0	-37.2	-148.8	142.8	-131.2
M-IV	-96.0	-51.7	-167.6	163.3	-147.1

The interaction energy of selected molecular pairs (from the .mlc file), extracted from the crystal packing along with the involved intermolecular interactions are listed in Table 7, with the total energies being partitioned into their coulombic, polarization, dispersion and repulsion contributions. The molecular pairs are arranged in decreasing order of their stabilizing energies. As it is shown in the Table 6 that energies of molecule M-I and M-IV and that of M-II and M-III are comparable and the molecules M-II and M-III are more stable than M-I and M-IV. The combined nature of the interaction is predominately in all the four molecules is dispersive. The geometrical restrictions placed on the intermolecular H-bonds present in the selected molecular pairs are the sum of the Vander Waals radii + 0.3 Å and the directionality is greater than 110º. A precise description of each molecule with regard to its energy contribution and molecular pair formation is presented:

(M-I) 2-hydrazinyl benzo[d]thiazole

All the molecular pairs (I-IV) extracted from the crystal packing are shown in the Fig.2 having an interaction energy of -72.7 kJ mol^{-1}. The most stabilizing molecular pair shows the presence of N-H…N hydrogen bonding which leads to the formation of $R^2_2(8)^{21}$ graph-set motif. The second most prominent interaction in this case is three centered bifurcated N-H...C hydrogen bonding with N1- H21 act as a donar for both the acceptor elements C1 and C7.

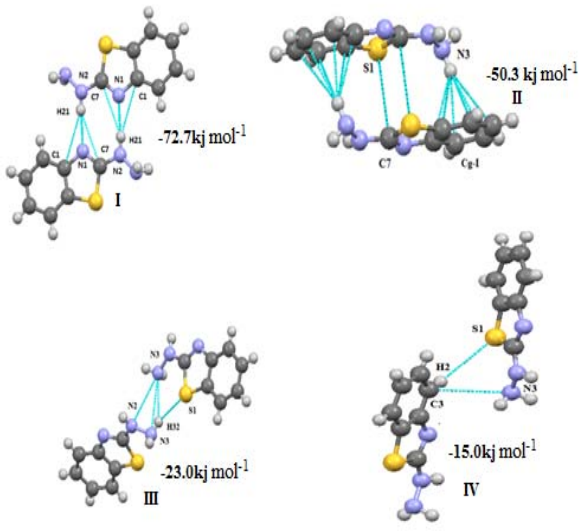

Figure 2. M-I: Molecular pair formations with their interaction energy contributions

The second most stabilized molecular pair in the crystal structure, formed via C-H…Cg-I molecular interactions (Cg-I is Centeroid of ring C1/C2/C3/C4/C5/C6), has a contribution of -50.3 kJ mol^{-1} (50% contribution to stabilization from the dispersion energy) to the stabilization of the packing. These molecular stacks are interlinked via weak N-H…S, S-H…N bonding (motif III,-23.0 kJ mol^{-1}) and C-H…S and C2-N3 (motif IV, -15.0 kJ mol^{-1}) intermolecular hydrogen respectively.

(M-II) 6-Chloro-5-fluoro-2-hydrazinyl benzo[d]thiazole

All the molecular pairs (I-VI) extracted after the PIXEL calculation are represented in Fig.3 along with their interaction energies. In this molecule the hydrogen atoms at the position 3 and 4 are replaced by Chlorine and Fluorine element.

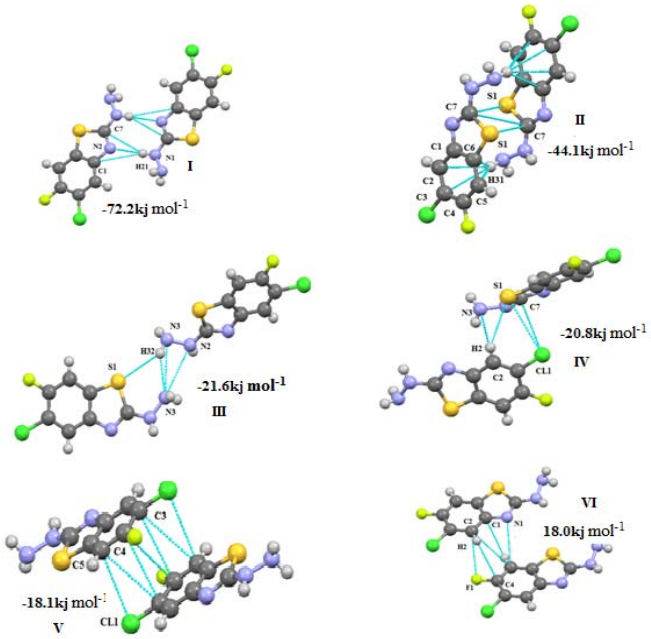

Figure 3. M-II: Molecular pairs along with their interaction energies

Here motif I is the most stabilized pair with an interaction energy of –72.2 kJ mol^{-1} in the crystal packing and consist of interaction involving H21 atom in three hydrogen bonds [N-H…C (involving H21 with C1 and C7) and N1-H21…N2] leads to the bifurcated hydrogen bonding. The nature of the interaction is governed by the couloumbic and repulsive energy with their maximum contribution to total stabilization energy. The motif II is the second most stabilized pair with interaction energy -44.1kJ mol^{-1} involving weak N-H…Cg-I(Cg-I is Centeroid of ring C1/C2/ C3/C4/C5/C6) N…N and N-H…S interactions. In rest of the motifs of this molecule the nature of the stabilized energy is predominately dispersive as this part of the energy contributes more than 70% to the total interaction energy except motif-IV (to which its contribution is around 40%), with energy interaction ranges from -18.0 to -24.8 kJ mol^{-1}. In these motifs the structure is stabilized by weak C-H…C, C-H…S, C…C, C…F, N…C and C...Cl interaction.

(M-III) 2-hydrazinylmethyl benzo[d]thiazole

The important packing motifs (I-III) extracted from crystal packing along with their stabilization energies are shown in Fig.4. Among all the three motifs stabilization energies are comparable with their values being -40.8, -34.8 and -30.1 kJ mol^{-1} respectively Table 7.

Table 7. PIXEL interaction energies (I. E.) kJ mol^{-1} between molecular pairs related by a symmetry operation and the associated molecular interaction in the crystal

Motifs	Centroids distances	E_{coul}	E_{Pot}	E_{Disp}	E_{Rep}	E_{Tot}	Symmetry	Important interactions
M-I								
I	6.248	-98.0	-44.3	-35.9	105.5	-72.7	1-x, 1-y, 2-z	N2-H21…N1 N1-H21…C1 N2-H21…C7 N2…N1
II	4.190	-25.8	-20.7	-53.8	50.0	-50.3	1-x, -y, 2-z	S1…C7 N3-H31…π
III	10.730	-71.8	-6.3	-4.0	15.1	-23.0	-1/2-x, ½+y, 2.5-z	N3-H32…N3 N3-H32…S1 N3…N3, N3…N2
IV	7.130	-6.3	-2.8	-15.5	9.7	-15.0	-2/2+x, ½-y, -1/2+z	C3-H2…S1 C3-N3
M-II								
I	7.727	-92.2	-44.3	-34.6	99.0	-72.2	-x, -y, -z	N1-H21…N2 N1-H21…C1 N1-H21…C7 N1…N2
II	5.743	-23.7	-23.5	-59.7	62.5	-44.1	-x, 1-y, -z	S1-H31…π S1…C7, C1-C7
III	10.730	-18	8.4	17.0	22.6	-20.8	x, ½+y, ½	N3-H32…S1 N3-H32…N3 N3…N3, N3…N2
IV	7.076	-6.1	-4.7	-26.5	18.8	-18.5	x, ½-y, ½+z	C2-H2…S1 C2-H2…N3 CL1-C7 CL1-S1
V	5.462	-3.9	-2.8	-32.6	21.3	-18.0	1-x, 1-y, -z	C4…C3, C3…C5 C4…C4, CL1-C5
VI	5.664	-0.2	2.8	-21.7	11.6	-13.0	x, -1+y, -z	C2…C5, C2…F1 N1…C5 C5-H5…C1 C5-H5…C1
M-III								
I	7.810	-37.1	-13.0	-24.0	33.3	-40.8	2-x, -1/2+y, 1-z	N2-H21…S1 N2-H21…N3 N2…N3, N1…N3 C7…N3
II	7.150	-31.0	-13.3	-23.2	32.8	-34.8	1-x, -1/2+y, 1-z	N3-H32…C7 C6…C1 C8-H8B…C8
III	6.4	-14.6	-12.4	-54.5	51.4	30.1	-1+x, y, z	C1…C6 C8-H8B…C8 S3-H32…C7

M-IV [A...B]								
I	7.754	-95.9	-46.0	-34.9	104.8	-71.9	½+x, 2-y, z	N2A-H21A…NIB N2B-H21B…N1A N2A-H21A…C7B N2B-H21B…C7A N1A-N2B, N2A…N1B
II	5.448	-26.8	-22.2	-57.2	59.5	-46.6	½+x, 1-y, z	N3B-H32B… π N3A-H32A… π S1A…C7B, C7A-S1B
III	9.946	-21.2	-8.6	-18.0	24.2	-23.6	x, y, z	N3B-H2B…S1A N3B-H2B…N3A N2B-N3A
IV	10.037	-16.7	-7.0	-16.7	18.9	-21.6	x, 1+y, z	CL1B… π C1A, C4A C5A, C6A
V	6.443	-3.2	-3.1	-24.8	16.2	-14.9	1-x, 1-y1/2+z	CL1A…C1B CL1A…C6B C3A-H3A…CL1B C3A-H3A…C4B
VI	7.101	-3.5	-1.8	-14.3	6.5	-13.1	½-x, y, ½+z	CL1A…H3B
M-IV [A....A]								
I	7.085	-7.4	-4.3	-19.2	14.2	-16.7	-1/2+x, 1-y, z	C2A…H2A-N3A N3A-H31A…C1A C2A-H2A…S1A S1A…C2A N3A…C2A
II	5.777	-2.5	-3.3	-22.8	13.4	-15.2	x, -1+y, 2-y	CL1A…C2A C2A…C5
M-IV [B…B]								
I	6.966	-7.5	-4.5	-20.2	15.9	-16.2	-1/2+x, 1-y, z	C2B…SIB N3B…C2B C2N-H2B…S1B
II	5.777	-1.4	-2.8	-21.8	11.3	-14.7	x, y-1, z	CL1B…C2B C5B… C2A

In the first two motifs the maximum stabilization energy comes from the coulombic part where as the motif-III is stabilized by the dispersive energy as in this case it contributes more than 50% to the total stabilization energy. The motif-I is stabilized due to the presence of weak N-H…S and N-H…N (H21, N2, N3 & S1) interaction. It also involves the N1...N3, N2…N3 and N3…C7 interaction. The next two stabilized molecular pairs (II and III) involve C-C molecular stacking, however along with this interaction the motif-II shows the presence of N-H…C where as motif-III is shows the presence of N-H...N hydrogen bonding.

(M-IV) 5-chloro-2-hydrazinyl benzo[d]thiazole

The different structural motifs (I-X) contributing towards the crystal packing are shown in Fig.5a, Fig.5b, Fig.5c. The molecule crystallizes with two molecules in the asymmetric unit [molecule A (carbon atom = grey colour) and B (carbon atom = violet colour)]. In this compound, there exist three types of molecular pairs A–A, A–B and B–B, respectively. Energetically A–B type molecular pairs are more stable than the A–A and B–B type.

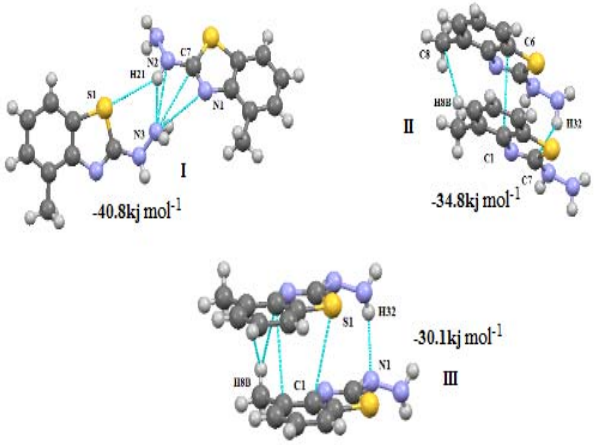

Figure 4. M-III: Molecular pair formations with their interaction energy contributions

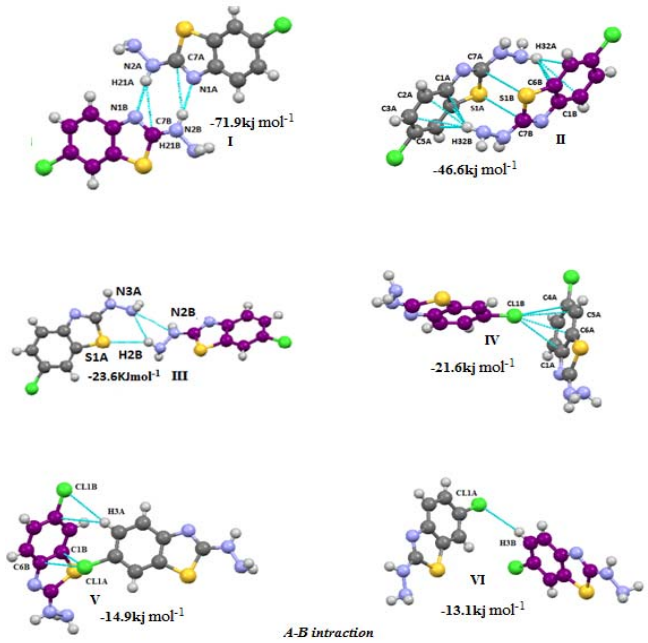

Figure 5a. M-IV: Molecular pair formations with their interaction energy contributions

(i) A-B interaction motifs

The two molecules in the asymmetric unit are packed with the involvement of dimeric interactions represented by the graph set motif $R^2_2(8)$ formed with a strong N-H…N and weak N-H…C (involving N1B and C7B with bifurcated donar pair N2A-H21A) hydrogen bonds and this pair is the most stabilized pair in the crystal, energy being -71.9 kJ mol^{-1} and the principal stabilization of around 50% corresponding to coulombic component. The second most stabilized molecular pair (motif II) in the crystal structure is stacked via N-H…π interaction involving N3-H32 and benzene ring of both the asymmetric unit A and B along with C...S interactions and has a contribution of -46.6 kJ mol^{-1} to the stabilization of the crystal packing. In motif-III the two asymmetric units A and B are connected by bifurcated N3B-H32B…S1A and N3B-H32B…N3A hydrogen bonding with N3B-H32B acts as a common donar to both the elements. This interaction has maximum contribution from coulombic and repulsive part with total stabilization energy of value -23.6 kJ mol^{-1}. In rest of these motifs the two symmetry units are linked through the weak bonding involving chlorine atom with C3B-CL1B…π in motif-IV[where π is the centeroid of the benzene ring of molecule A in the asymmetric unit], bifurcated hydrogen bonding in motif-V [involves C3-H3… Cl1 in both the symmetric units A and B] represented by the graph set motif $R^4_2(8)$ and C3B-H3B…CL1A hydrogen bonding in the case of motif VI.

(ii) A-A interaction motifs

The two important motifs (I, II) showing the interaction between the two similar molecules (A, A) in the asymmetric unit are extracted from crystal packing along with their stabilization energies are represented in the Fig. 5b. Both these interactions motifs are dispersive in nature as it contributes maximum to the total stabilization energies -16.7 and -15.2 kJ mol^{-1} in case of motif I and II respectively. The motif I is stabilized with the presence of C2A-H2A…S1A, S1A…C2A and N3A…C2A and motif II shows the involvement of C3A-Cl1A…C2A and C5A…C2A for the stabilization of the molecular packing.

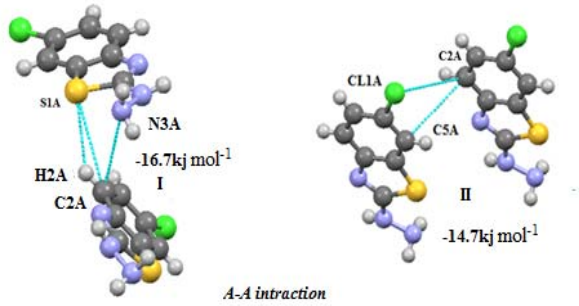

Figure 5b. M-IV: Molecular pair formations with their interaction energy contributions in A-A interaction

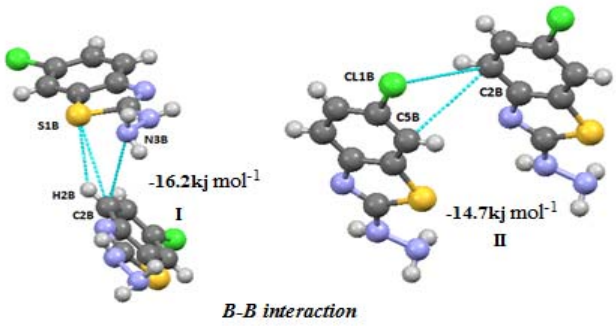

Figure 5b. M-IV: Molecular pair formations with their interaction energy contributions in B-B interaction

(iii) B-B interaction motifs

Molecular pairs (I, II) extracted from M-IV along with their respective interaction energies are shown in Fig. 5c. The packing features of motif I and II are almost identical to

the motif I and II respectively in A-A interaction and results in the generation of similar packing motifs. In this case the energies are predominately dispersive in nature with the total energy values -16.2 and -14.7 kJ mol^{-1} in motif I and II which are quite similar as we have seen in above described A-A interactions.

Conclusions

An analysis of the energetics of the neighbouring molecular pairs of four thiazole derivatives shows the presence of different intermolecular interactions participating in the crystal packing. The total interaction energy among different molecular pairs has been divided into corresponding coulombic, polarization, dispersion and repulsion contribution which facilitates a better understanding of the nature of intermolecular interactions contributing towards the crystal packing. The dispersive energy contributes maximum to the stabilization of the structure in all the four molecules. Hence the combined nature of the interaction energy in all the four molecules is predominately dispersive. It has been found that N-H...N hydrogen bonds plays an important role in the stabilization of the crystal packing. Along with these hydrogen bonds, N-H...π, C-H...S and N....N interaction has also become the important linkage in most of the molecular pairs. It is of interest to extend this evaluation of energies of molecular pairs in other thiazole derivatives which will enable us to have better understanding of weak intermolecular interactions.

Acknowledgement

One of the authors (Rajni Kant) acknowledges the Department of Science & Technology for single crystal X-ray Diffractometer as a National Facility under Project No. SR/S2/CMP-47/2003 and DST Project No: EMR/2014/000467. RS acknowledges University Grant Commission (UGC) for the award of NET-JRF scholarship under ref. No. 23/12/2012 (ii) EU-V.

References

[1]Liu, X. F., Liu, X.-H., *Acta Cryst.,* **2011**, *E67*, o202.

[2]Liu, X. H., Tan, C. X., Weng, J. Q., *Phosphorus Sulfur Silicon Relat. Elem.,* **2011a**, *186*, 552-557.

[3]Liu, X. H., Tan, C. X., Weng, J. Q., *Phosphorus Sulfur Silicon Relat. Elem.,* **2011b**, *186*, 558-557.

[4]Yaseen, A., Haitham, A. S., Houssain, A. S., Najim, A., *Z. Naturforsch. Teil B.*, **2006**, *62* 523–528.

[5]Kini, S., Swain, S. P., Gandhi, A. M., *Indian J. Pharm. Sci.,* **2007**, *69*, 46–50.

[6]Munirajasekhar, D., Himaja, M., Sunil, V. M., *Int. Res. J. Pharm.,* **2011**, *2*, 114–117.

[7]Gurupadayya, B. M., Gopal, M., Padmashali, B., Manohara, Y. N., *Indian J. Pharm. Sci.,* **2008**, *70*, 572–577.

[8]Gavezzotti, A., *New J. Chem.,* **2011**, *35*, 1360-1368.

[9]Sharma, R., Prakash , S. N., Narayana, B., Gupta, V.K., Kant, R., *Eur Chem. Bull.,* **2014**, *3(4),* 337-339.

[10]Hoong-Kun, F., Ching, K. Q, Sarojini, B. K., Mohan,B. J., Narayana, B., *Acta Cryst,.,* **2012**, *E68*, o2459.

[11]Xu-Feng, L., Xiao-Yong, Y., Shao-Liang, J., *Acta Cryst.,* **2011**, *E67*, o1641.

[12]Hoong-Kun, F., Chin W. O., Sarojini., B. K., Mohan, B. J., Narayana,B., *Acta Cryst.,* **2012**, *E68*, o691–o692.

[13]Burke-Laing, M., Laing, M., *Acta Cryst.,* **1976**, *B32*, 3216-3224.

[14]Allen, F. H., Kennard, O., Watson, D. G., Brammer, L., Orpen, A. G.,Taylor, R.., *J. Chem. Soc. Perkin Trans.,* **1987**, *2,* S1–19.

[15]Fun, H.-K., Arshad, S., Himaja, M., Munirajasekhar, D., Sarojini, B. K., *Acta Cryst.,* **2011a,** *E67*, o2412.

[16]Taylor, R., Kenard, O., *J. Am. Chem. Soc*., **1982**, *104*, 5063-5070.

[17]Hunter, C. A., Sanders, J. K. M., *J. Am. Chem. Soc.,* **1990***, 112,* 5525-5534.

[18]Desiraju, G. R., Steiner, T., *The Weak Hydrogen Bond* in *Structural Chemistry and Biology*, **1999**, Oxford University Press, Oxford.

[19]Calhorda, M. J., *Chem. Commun..,* **2000**, 801-809.

[20]Dunitz, J. D., Gavezzotti, A., *Cryst. Growth Des.,* **2005,** *5*, 2180-2189.

[21]Bernstein, J., Davis, R. E., Shimoni, L., Chang, N.L., *Angew. Chem. Int. Ed. Engl.,* **1995**, *34,* 1555–1573.

Received: 12.06.2015.
Accepted: 08.07.2015.

METABOLIC FATE OF [^{14}C]GLUCOSE IN PERICARPS AND SEEDS OF *COFFEA ARABICA* AND *COFFEA CANEPHORA* FRUITS DURING DEVELOPMENT AND RIPENING

Yukiko Koshiro[a], Chifumi Nagai[b] and Hiroshi Ashihara[a]*

Keywords: carbohydrate, biosynthesis, metabolism, *Coffea arabica*, *Coffea canephora*.

To elucidate the overall metabolism of sugars in coffee fruits, in situ metabolism of exogenously supplied ^{14}C-glucose were investigated in segments of pericarps and seeds of two cultivars of *Coffea arabica* and *C. canephora* fruits obtained from different growth and ripening stages. The coffee fruits were categorized into five stages 1 to 5 which were corresponding to young, developing, mature (green), ripening (pink) and fully-ripened (red) fruits, respectively. The rates of uptake and metabolism of [U-^{14}C]glucose in fruits of the stages 1–3 was higher than in fruits of stages 4–5. Release of $^{14}CO_2$ which represented cellular respiration was high in both pericarp and seeds of *C. arabica* and *C. canephora* up to the stage 3, but it gradually reduced and the minimum was found in the fully ripened stage 5 fruits. The highest incorporation of radioactivity into the methanol-soluble metabolites was found in the stage 2 fruits. In pericarp, incorporation of radioactivity into the acidic component (mainly consisted of organic acids) was much higher than into basic component (mainly consisted free amino acids). In seeds, significant amounts of the radioactivity were found in the basic fractions especially at the stages 4 and 5. [U-^{14}C]glucose was converted to fructose and sucrose in both pericarp and seeds. Only small rate of sucrose synthesis from [^{14}C]glucose was detected 18 h after administration, however, its relative rate is slightly increased at stages 4-5 fruits. Incorporation of radioactivity into the methanol-insoluble metabolites (mainly consisted protein starch and cell wall constituents) was found in any stages of fruits. The maximum rates were found in pericarp and seeds of developing (stage 2) fruits of *C. arabica* and in those at early three stages 1–3 of *C. canephora*. Possible metabolic routes and relative participation of carbon in different metabolite biosynthesis in coffee fruits are discussed.

*Corresponding Author
Fax: +81-3-5700-4225
E-Mail: ashihara.hiroshi@ocha.ac.jp
[a] Department of Biology, Ochanomizu University, Tokyo, 112-8610, Japan
[b] Hawaii Agriculture Research Center, Kunia, Hawaii 96759, USA

Introduction

Coffee is a useful plant and many studies on its metabolites have been performed using coffee beans (seeds) from the view points of food chemistry and human health.[1-3] However, little is known on biosynthesis and metabolism of these metabolites in coffee plants. As a part of the series of our research to elucidate the primarily and secondary metabolism in coffee fruits, we have earlier investigated the biosynthesis of caffeine, trigonelline and chlorogenic acids in growing and ripening fruits of *Coffea arabica* and *Coffea canephora*.[4,5] In this subsequent study, we have examined carbohydrate metabolism in coffee fruits using *C. arabica*, cv. Mokka and cv. Catimor and *C. canephora* grown in the coffee field of the Hawaii Agriculture Research Center, Oahu Island.

In coffee plants, atmospheric CO_2 is fixed by photosynthesis mainly in leaves and a photosynthate, sucrose, appeared to be translocated to the sink including coffee fruits. In addition, limited amounts of CO_2 are also fixed at the surface of pericarps and translocated to seeds. Sucrose synthesized in leaves is loaded into phloem by the H^+-sucrose co-transporter. Loaded sucrose is translocated to fruit flesh through the phloem and is unloaded into the parenchyma tissue.[6] In the sink, sucrose is converted to monosaccharides and then metabolised. Geromel et al.[7,8] reported that invertase activity was high during early stage of coffee fruits and sucrose was hydrolysed to glucose and fructose. Therefore, in order to investigate the profile of sugar metabolism in pericarps and seeds during growth of coffee fruits, we have applied [U-^{14}C]glucose to the segments of pericarps and seeds and followed the metabolic fate. On the basis of the results obtained, overall sugar metabolism in coffee fruits has been discussed.

Experimental

Plant Material

Fruits of *Coffee arabica* cv. Mokka (MA2-7) and cv. Catimor (T5175-7-1), and of *Coffea canephora*, were obtained from the Experimental Station of Hawaii Agriculture Center, Kunia Station, Oahu Island, Hawaii. These coffee trees were cultivated at the same site at an altitude of ca. 150 m above sea level. Fruits were divided into five stages according to the growth and maturity of coffee fruits.

Radiochemicals and biochemicals

[U-^{14}C]Glucose (specific activity 9.1 GBq mmol^{-1}) was purchased from Moravek Biochemicals Inc, Brea, CA, USA. Standards of metabolites were purchased from Sigma-Aldrich, St. Louis, Mo, USA.

Administration and Analysis of ^{14}C-labelled Glucose

Administration and analysis were according to the methods described in our earlier papers[9-12] with slight modifications. Samples (~100 mg fresh weight) and 2.0 mL of 20 mM sodium phosphate buffer (pH 5.6) containing 1 mM [U-^{14}C]glucose and 0.5 % sodium ascorbate were placed in the main compartment of a 30-ml Erlenmeyer flask. The flask was fitted with a small glass tube that contained a piece of filter paper impregnated with 0.1 mL of 20% KOH in the centre well, to collect $^{14}CO_2$. Each reaction was started by adding a solution of the radioactive compound to the main compartment. The flasks were incubated for 18 h in an oscillating water bath at 27 ºC. After incubation, the plant materials were harvested using a stainless steel tea strainer, then washed with distilled water and frozen with liquid nitrogen. They were then stored at -80 ºC. Potassium bicarbonate that had been absorbed by the filter paper was allowed to diffuse into distilled water overnight, and aliquots of the resulting solution (usually 0.5 mL) were used for determination of the radioactivity with a liquid scintillation analyser.

The frozen plant materials were homogenized in 80 % methanol using a pestle and mortar. The homogenates were centrifuged at 12,000 x g for 10 min. The resulting supernatant was collected and the precipitate was re-suspended with 80 % methanol, and the supernatant was collected by centrifuging. The first and second methanol-soluble fractions were combined. After complete evaporation of the methanol, the methanol-soluble extracts were dissolved in distilled water. The methanol-soluble fraction were fractionated into sugars, amino acids and organic acids on two types of ion-exchange resins, Dowex 50W-X8 (H^+ form) and Dowex 1-X8 (Cl^- form).

The basic components including free amino acids and the acidic components including organic acids were eluted with 2 N NH_4OH from the Dowex 50W-X8 column and 5N HCO_2H from Dowex 1-X8 (Cl^- form), respectively. The neutral components including sugars were obtained in the effluent from the two columns.

Sugars were separated by TLC using butanol-acetic acid-water (4: 1:2 v/v) as the developing solvent. Development was repeated after drying to complete the separation.

Results and Discussion

Growth Stages of Coffee Fruits during Development and Ripening

In this paper, the five growth stages of coffee fruits from the sizes and maturation are defined. Fruits of stages 1 to 3 are green-coloured ones of small, medium and large sizes. They are roughly corresponded to the rapid expansion and pericarp growth stage, the endosperm formation stage and the dry matter accumulation stage as described by Cannell.[13] At stage 4, fruit skin colour was changed from green to pink and seeds were pre-ripened, and at stage 5, colour was changed to red and seeds are fully ripened. Fresh weights and sizes of fruits in stages 1 to 5 are shown in Table 1.

Metabolic Fate of [^{14}C]Glucose

In order to examine the metabolic fate of [U-^{14}C]glucose which is taken up by the segments of pericarps and seeds of coffee fruits, respiratory released $^{14}CO_2$ was collected with KOH in the centre well of the incubation flasks and intracellular ^{14}C-metabolites were extracted with 80 % methanol and the methanol-soluble and methanol-insoluble components were obtained.

Table 1. Growth stages and fresh weights of Coffee fruits.

Sample	Stage	Colour	Fresh weight (mg)
Coffea arabica	1	Green	215± 3
cv. Mokka	2	Green	822±16
	3	Green	915±14
	4	Pink	1037±40
	5	Red	1180± 9
Coffea arabica	1	Green	236± 4
cv. Catimor	2	Green	800±35
	3	Green	849±41
	4	Pink	1012±39
	5	Red	1288±11
Coffea canephora	1	Green	239±11
	2	Green	545± 3
	3	Green	622± 7
	4	Pink	778±73
	5	Red	1112±90

The compounds in the methanol-soluble components were fractionated by ion-exchange and thin-layer chromatography as illustrated in Figure 1.

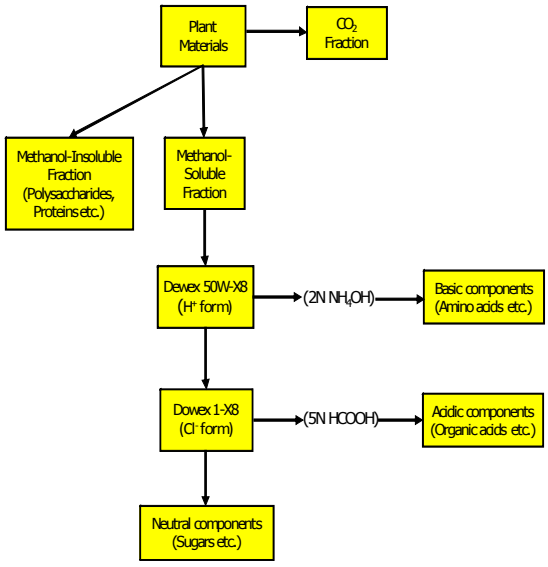

Figure 1. Flow sheet of the separation of ^{14}C-labelled metabolites

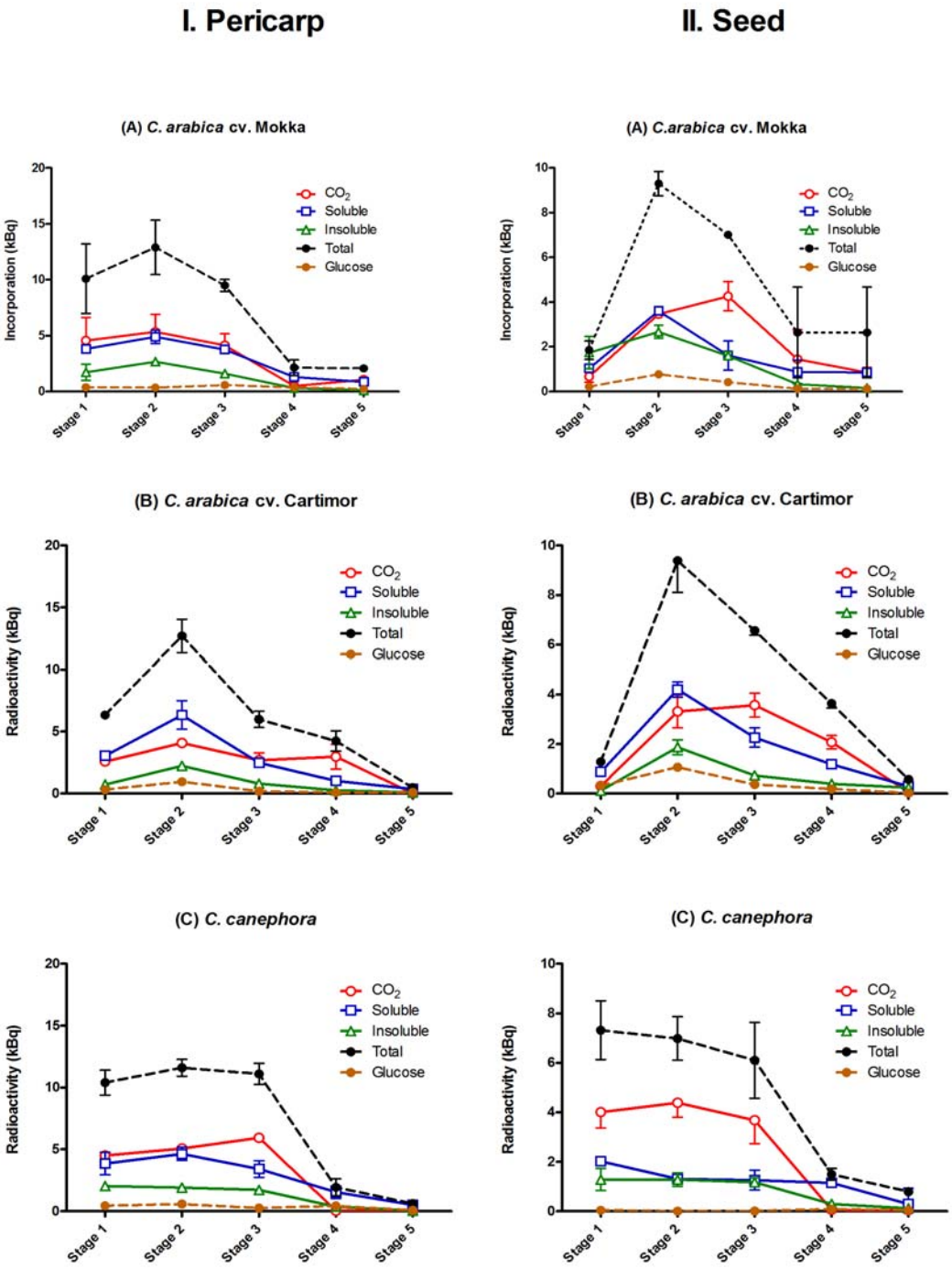

Figure 2. Changes in the incorporation of radioactivity from [U-^{14}C]glucose into CO_2, methanol-soluble and methanol-insoluble components.

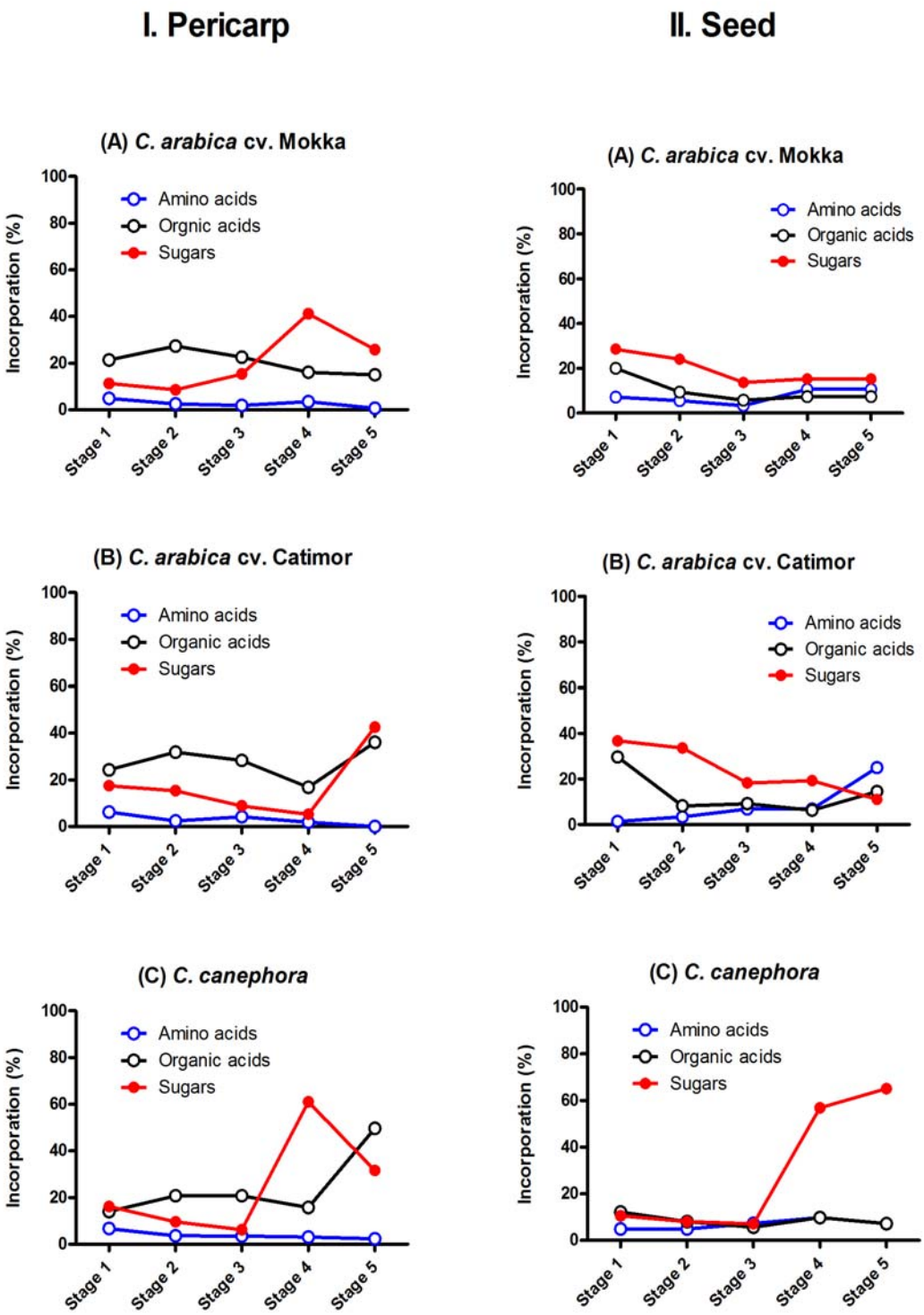

Figure 3. Distribution of the radioactivity from [U-^{14}C]glucose in the methanol soluble metabolites during growth. Incorporation into amino acids, organic acids and sugars is shown as % of total uptake shown in Figure 2.

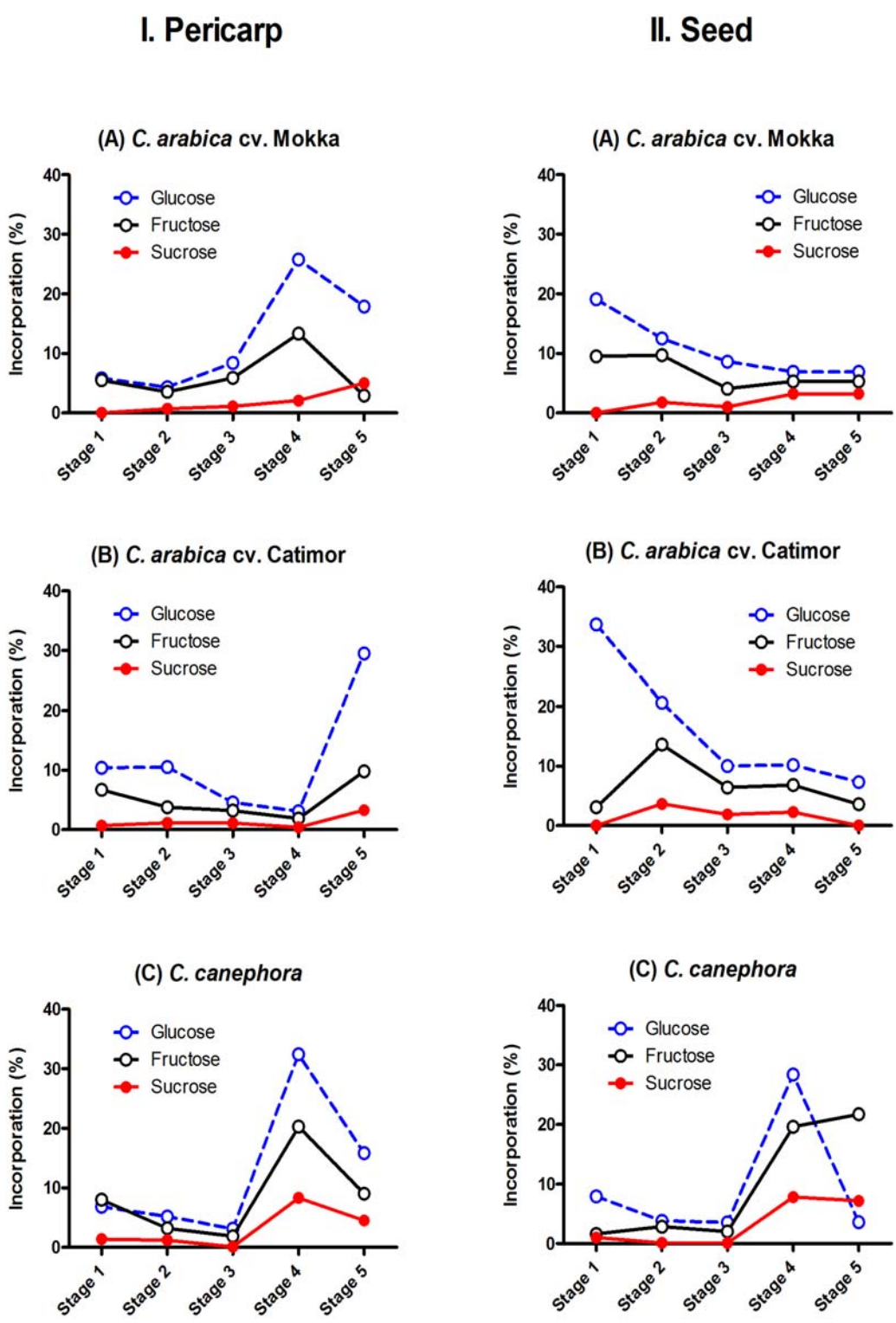

Figure 4. Incorporation of the radioactivity from [U-^{14}C]glucose into individual sugars during growth. Distribution of radioactivity in glucose, fructose and sucrose is shown as % of total uptake shown in Figure 2.

The total uptake of [U-^{14}C]glucose by the segments of pericarps and seeds of three coffee samples and incorporation of radioactivity into CO_2, methanol-soluble and methanol-insoluble fractions are shown in Figure 2. The radioactivity detected in glucose, some of which may be unmetabolized precursor, is also shown for reference. Since most of applied [U-^{14}C]glucose were metabolized and not retained in the tissues, uptake rates of [^{14}C]glucose seems to be directly related to the metabolic capacity of each tissue. In pericarps of *C. arabica* cv. Mokka, the rates of total uptake of [^{14}C]glucose during 18 h incubation in the fruits of stages 1–3 were 10–13 kBq/100 mg FW, but the rates reduced to ~2 kBq at the stages 4–5. Although slight difference was found (for example, higher value at stage 4 of *C. arabica* cv. Catimor), but the pattern of three coffee samples essentially resembled. Thus, in coffee pericarp, activity of glucose metabolism is active during development and is reduced on the ripening of the fruits.

The pattern of [^{14}C]glucose uptake in seeds was different between *C. arabica* and *C. canephora*. The rates of total uptake of [^{14}C]glucose in stage 1 seeds of *C. arabica* cv. Mokka and cv. Catimor were low (1.9 and 1.3 kBq/100 mg FW, respectively), and then increased at stage 2 (9.3 and 9.4 kBq, respectively) and after that they were gradually reduced. In contrast, the total uptake of [^{14}C]glucose was high in stages 1–3 of *C. canephora* seeds (6.1–7.3 kBq) and then decreased rapidly.

The incorporation of ^{14}C into CO_2, methanol-soluble and methanol-insoluble cellular components were examined. Most of CO_2 is released by the catabolic pathway of glucose, namely glycolysis and the tricarboxylic acid (TCA) cycle. In general, 35–60 % of glucose taken up by the tissues was catabolised in both pericarps and seeds. The respiratory glucose catabolism of exogenously supplied [^{14}C]glucose was markedly reduced in the ripening of fruits. Incorporation of ^{14}C into the methanol-soluble metabolites is usually higher than in methanol-insoluble metabolites. For example, in *C. arabica* cv. Mokka of green pericarps (Stages 1–3), 41–44 % of the total radioactivity was released as CO_2, 38–40 % of radioactivity was recovered as methanol-soluble fraction and the rest (17–21 %) was incorporated into methanol-insoluble fraction. No significant difference was found between in pericarp and in seeds, respectively 37–55 %, 33–56 % and 8–24 % of total radioactivity was found in CO_2, methanol-soluble and methanol-insoluble fractions of *C. arabica* cv. Mokka seeds of the stages 1–3.

Incorporation of radioactivity from [^{14}C]glucose into the methanol insoluble fraction usually occupied 10–20 % of total radioactivity. In this fraction mainly consisted of proteins and polysaccharides including starch and cell wall constitutes.[10] Special galactomannans and arabinogalactan polysaccharides of coffee seeds seem to be also included in this fraction.[14]

The methanol-soluble fraction was separated into three components using ion-exchange chromatography. Major components of the basic, acidic and neutral fractions of [^{14}C]glucose metabolism are amino acids, organic acids and sugars.[9] Therefore, data obtained in this study are shown as amino acids, organic acids and sugars and the values are presented as % of total radioactivity taken up by the samples (Figure 3). The radioactivity incorporated into amino acids was lower than that into organic acids, except for the later stages of seeds; the relative incorporation into amino acids (25 %) was higher than that into organic acids (15 %) in the stage 5 of *C. arabica* cv. Catimor seeds.

The neutral fraction was further analysed by TLC and found that most radioactivity was distributed in glucose, fructose and sucrose and the radioactivity located in other unidentified spots was extremely low (data not shown).

Changes in the distribution of radioactivity from [^{14}C]glucose into these three sugars are shown as % of total radioactivity taken up by the segments and shown in Figure 4. The radioactivity found in glucose may be mainly due to the unmetabolized glucose. The values were high in the later stages of pericarps in all coffee plants and the stage 1 of seeds of two cultivars of *C. arabica*. In general, radioactivity recovered in fructose was higher than in sucrose. Incorporation of radioactivity into sucrose from [^{14}C]glucose was detected both in pericarp and in seeds. The rates were slightly increased with the ripening of fruits. However, the activity of sucrose biosynthesis in pericarp and seeds of coffee fruits was restricted.

In situ metabolism of exogenously supplied [U-^{14}C]glucose suggests that possible metabolic pathways illustrated in Figure 5 are operative in pericarps and seeds of coffea plants. Glucose is converted to glucose-6-phosphate (G6P) and enters to the glycolytic pathway and then metabolised by the TCA cycle. In these processes, $^{14}CO_2$ is released at the steps of pyruvate dehydrogenase, isocitrate dehydrogenase and 2-oxoglutarate dehydrogenase. The results of current studies indicate that active glycolysis and subsequent respiration occur during the development of fruits and its activity decreased with ripening the fruits. This is probably due to the fact that ATP is required for the development of coffee fruits. Organic acids, such as malate and citrate, are the members of the TCA cycle. Probably these two compounds are the major ^{14}C-metabolites during short (18 h) incubation as shown in other plant materials.[10] Considerable radioactivity from [U-^{14}C]glucose may be incorporated into amino acids via 2-oxoglutarate and then incorporated into proteins.[9] [U-^{14}C]glucose is utilized for the synthesis of sucrose and polysaccharides including cell wall constitutes and starch via UDP- and ADP-glucose.[14]

Coffee seeds accumulate sucrose (4–8 % dry weight), caffeine (1–2 %), chlorogenic acids (6–10 %), trigonelline (0.7–1 %) and polysaccharides (45–50 %).[15] However, little or no radioactivity from [U-^{14}C]glucose into these compounds was detected 18 h after administration. This may reflect that the distance of the pathway from glucose was long and biosynthetic velocity of these compounds is rather slow compared with the primary metabolites which turnover is fast. These secondary metabolites and storage compounds are gradually accumulated.

In conclusion, carbohydrate metabolism in young developing fruits is active and reducing sugars, such as glucose, are utilized for energy metabolism to produce ATP. Large portion of carbon-skeleton of sugars are released as CO_2 by respiratory metabolism, i.e., glycolysis and the TCA cycle, and the rest was utilized for the synthesis of organic acids, amino acids and sugars. These precursors are gradually converted to the storage compounds which are accumulated in coffee seeds.

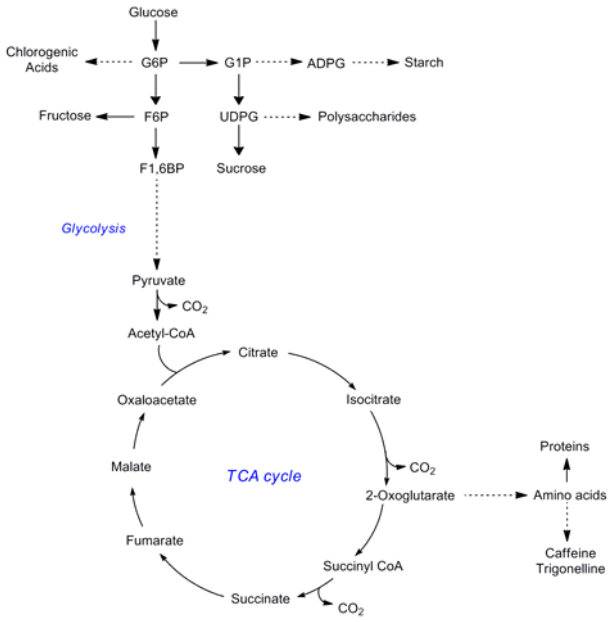

Figure 5. Possible metabolic routes of [^{14}C]glucose in pericarps and seeds of *Coffea arabica* and *C. canephora*. ADPG, ADP-glucose; F6P, fructose-6-phosphate; F1,6BP, fructose-1,6-bisphosphate; G1P, glucose-1-phosphate; G6P, glucose-6-phosphate; UDPG, UDP-glucose.

Acknowledgements

The authors thank Dr. Riko Katahira, Kobe Shoin Women's university for her valuable comments on this manuscript.

References

[1]Clarke, R.J. and Vitzthum, O.G., *Coffee Recent Development*, Blackwell Science, **2001**, 1-257.

[2]Crozier, A., Ashihara, H., and Tomas-Barberan, F., *Teas, Cocoa and Coffee: Plant Secondary Metabolites and Health*, Wiley-Blackwell, **2012**, 1-252.

[3]Ludwig, I.A., Clifford, M.N., Lean, M.E.J., Ashihara, H. and Crozier, A., *Food Funct.*, **2014**, *5*, 1695-1717.

[4]Koshiro, Y., Zheng, X.Q., Wang, M., Nagai, C. and Ashihara, H., *Plant Sci.*, **2006**, *171*, 242-250.

[5]Koshiro, Y., Jackson, M.C., Katahira, R., Wang, M.L., Nagai, C. and Ashihara, H., *Z. Naturforsch.*, **2008**, *62c*, 731-742.

[6]Yamaki, S., *J. Jpn. Soc. Horticul. Sci.*, **2010**, *79*, 1-15.

[7]Geromel, C., Ferreira, L.P., Guerreiro, S.M.C., Cavalari, A.A., Pot, D., Pereira, L.F.P., Leroy, T., Vieira, L.G.E., Mazzafera, P. and Marraccini, P., *J. Exp. Bot.*, **2006**, *57*, 3243-3258.

[8]Geromel, C., Ferreira, L.P., Bottcher, A, Pot, D., Pereira, L.F.P., Leroy, T., Vieira, L.G.E., Mazzafera, P., and Marraccini, P., *Ann. Appl. Biol.*, **2008**, *152*, 179-187.

[9]Saito, M. and Ashihara, H., *Nat. Sci. Rep. Ochanomizu Univ.*, **1989**, *40*, 45-56.

[10]Ashihara, H. and Komamine, A., *Phytochemistry*, **1975**, *14*, 95-98.

[11]Sagishima, K., Kubota, K. and Ashihara H., *Ann. Bot.*, **1989**, *64*, 185-193.

[12]Ashihara, H. and Matsumura, H., *Int. J. Biochem.*, **1977**, *8*, 461-471.

[13]Cannell, M.G.R., *Coffee: Botany, Biochemistry and Production of Beans and Beverage*, Croom Helm, **1985**, 108-134.

[14]Redgwell, R. and Fischer, M., *Braz. J. Plant Physiol.*, **2006**, *18*, 165-174.

[15]Clarke, R. J., *Quality Control in the Food Industry, Volume 4, Second Edition*, Academic Press, **1987**, 161-191.

Received: 29.06.2015.
Accepted: 20.07.2015.

ASSESSMENT OF THE WORK-RELATED HEALTH STATUS OF IRON INDUSTRY WORKERS IN KULATHUR AT DINDIGUL DISTRICT

A. Pandia Rajan[a,b] and M. S. Dheena Dayalan[b]

Keywords: health hazards, foundry industry, hemoglobin count, total leukocyte count (TLC), differential leukocyte count (DLC).

Ecological contamination is a distressing issue at the present. It deals with every aspect of our life including birth to death. The problem is not from a pinpoint source; rather it is a wide problem which contains many more aspects beyond our imagination in air, water, land etc. Many types of health hazard are in our surroundings and they gradually exposed to us. Occupational exposure to harmful substance is a very important human health hazard Industrial empowerment worsts the problem. Check on polluting industries in Dindigul District at Kulathur. A person cannot avoid this type of health hazard. Foundry industry is strongly set at Kulathur and as such polluting the area and affect the life of nearby living persons and workers. Iron is the world's most commonly used metal and can usually be found with other elements in the form of steel. The frequently recorded health disorders between iron and steel industry workers includes: respiratory and skin problems as well as noise-related hearing impairment. An assessment has been done for the occupational hazard at iron foundry through haemoglobin concentration and total erythrocyte count. A decrement in total erythrocyte count (TLC) different Leukocyte count (DLC) and haemoglobin concentration (Hb conc.) has been found in foundry workers which is alarming to take rehabilitate steps.

Corresponding Authors
Tel: +91-9380939942
E-Mail: dr.msdchem@gmail.com
[a] Bharthiyar Univ., P. G. and Research, Department of Chemistry, G. T. N Arts College, Dindigul, India.
[b] P. G. and Research, Department of Chemistry, G. T. N Arts College, Dindigul, India

INTRODUCTION

Iron is the world's most commonly used metal and can usually be found with other elements in the form of steel.[1] Steel is not a single product, but more than 3,500 different products that have many different physical and chemical properties, 75 percent of which have been developed in the last 20 years.[2]

Foundry workers are exposed to a unique collection of environmental challenges including noise, heat, vibration, organic and inorganic chemical dusts, residue, aerosols, gases, acids and other pollutants. However, professionals in the field of occupational health have focused more on the adverse health effects resulting from exposure to physical factors. The physical loads, organizational factors, individual characteristics and psychosocial factors have been found to be related to various musculoskeletal symptoms, which consist of a multi-factorial mechanism of the work-related illness. Operations in the iron and steel industry may expose workers to wide range of hazards or workplace activities that could cause incidents, injuries, death, ill health or diseases.[3]

Pollutants emitted from foundry work cause so much damage to blood, which carries very innocently the harmful chemicals and gases to the various organs. These substances have been shown to produce harmful effects on the blood, bone marrow, spleen and lymph nodes, since blood cells. Toxic chemicals in the air are also stimulating the immune system to activate leukocytes and macrophages that can create tissue damage, especially to the cells living the blood vessels. Blood is an important factor for maintenance of better health.

The frequently recorded health disorders between iron and steel industry workers includes: respiratory (66 %), skin problems (31 %)[4,5] and noise-related hearing impairment.[6] Occupational dermatosis is any alteration in the skin, mucosa, and annexes, which is direct or indirectly caused, conditioned, maintained or aggravated by agents present in the occupational activity or work environment.[7] Therefore, present investigation has been made on the assessment of some haematological parameters in foundry workers at Kulathur in Dindigul District.

MATERIALS AND METHODS

There are about 10 permanent workers employed in the Iron industries. Out of this, 5 industrial workers who have been working for more than 20 years were selected for blood analysis.

The following were the “Criteria” followed for the inclusion for blood analysis.

- Those who were directly employed in rubber manufacturing operations.
- Those who have been working in the industrial units for more than ten years and above.
- Male workers in the age group of 40-60 years.

Table 1. The collected values of blood parameters of the foundry workers as given below

Blood Parameters		Standard value	Blood samples from the iron industry workers				
			S1	S2	S3	S4	S5
Age groups, years		40-60	47	55	43	50	44
Total leukocyte count, TLC, no. of cells mm^{-3}		4000-10000	8600	7400	9400	9900	10100
Differential leukocyte count, %	P	40-60	63	59	55	69	70
	L	20-40	31	40	40	30	25
	E	up to 6	3	2	5	1	5
	M	2-10	2	3	1	4	2
	B	up to 2	2	1	2	1	1
Erythro sedimentation rate (ESR), mm h^{-1}		5-20	25/50	15/30	10/20	10/20	10/20
Hemoglobin, g dL^{-1}		14-16	10.8	12.5	10.9	13.0	12.5
Total serum protein, g dL^{-1}			6.5	7.4	6.9	7.1	7.1
Albumin, g dL^{-1}			4.1	4.0	4.4	4.5	4.0
Globulin, g dL^{-1}			2.4	3.4	2.5	2.6	3.1
Albumin/globulin ratio			1.7	1.2	1.8	1.7	1.3

Samples: S1, woman, 47 old, S2- man, 55 years old, S3 – women, 43 years old, S4 – man, 50 years old, S5 – man, 44 years old. L: Lymphocytes B: Basophiles, E: Eosinophiles, P: Polymorphous, M: Monocytes

RESULTS AND DISCUSSIONS

In order to assess the health hazards associated with chemicals used in the Foundry industry Blood samples were collected from the persons in iron industry in order to diagnosis diseases like lungs disorder, gastro intestinal tract infection. Hexavalent chromium causes dermatitis, allergic skin reaction and skin veneration. The results obtained for the blood samples of the Iron workers Table 1.

Polymorphs

The polymorphs counts of the five samples are varied from 64 to 70 % but the normal value are 40-60 %. Here there is an increase of polymorphs from 64-70 % the indicating infection of the lungs to workers.

Lymphocytes

The Lymphocytes counts of selected samples are varied from 28 to 40 % and the normal values range from 28 to 40 % and the normal values range from 20 to 40 % indicating infective disease

Eosinophyles

The Eosinophile counts of the selected samples varied from 2 to 6 % but the normal values up to 6 % The result of the various blood samples of the foundry workers with age group of 40-46 are presented and discussed. From the Table 1 the following results obtained for various blood samples are discussed.

Total leukocyte count

The TC values for selected five samples varied from 8500 to 9800 cells mm^{-3} . Whereas the normal values range from 4000 to 10000 cells mm^{-3}. There results come under normal values.

Differential leukocyte count (DLC)

Differential count includes the percentage of polymorphs, lymphocytes, eosinophiles, monocytes and basophils.

Hemoglobin (Hb)

The Hb values of the given samples are varied from 7 to 10g/dL. But the normal values range from 14 to 16 g/dL. The deviation is due to Anaemia of the Foundry workers.

Total protein

The normal values of control samples is 6 to 8 g/L but the observed values for five samples are in the range of 6.8 to 7 g /L indicating the normal values of the workers.

These results are not within the standard limit. The deviation is due to allergic and asthma condition of the workers.

Monocytes

The monocytes of the selected samples are varied from 1 to 2 % and the normal values are 2 to 10 % and there is a decrease in monocytes due to tuberculosis infection.

Erythro sedimentation rate (ESR)

The ESR values of the five samples are varied from 15 mm for 1 h to 60 mm for 1 h but the normal values in 5 to 20 mm for 1 h. The deviation indicates the presence of tuberculosis among foundry workers.

Albumin

The normal albumin values range from 3.2 to 5 g dL^{-1} but the observed values for five samples range from 3.4 g dL^{-1} to 4.5 g dL^{-1}. The values are within the normal limit.

Globulin

The normal globulin values range from 2.3 to 3.6 g dL^{-1} but the experimental values for the five samples from 2.4 to 3.5 g dL^{-1} indicating the values are within the normal limit.

Albumin/globulin (A/G) ratio

The normal value of A/G ratio is 1 to 1.38. But the observed values are 0.9 to 1.8 indicating there is a deviation from the normal values indicating malnutrition of the foundry workers.

CONCLUSION

Working in iron and steel industry may be associated with higher prevalence of chest manifestations hearing impairment and other occupational diseases. The nature of the toxic chemicals handled within the iron industry itself is not good for the health of the workers bare handling of chemicals like metal dusts, acids, bases and other inorganic chemicals. Dust during various processes and chemical dust inhaled by the workers leading to bronchitis.

Workers are also exposed to various types of skin disease lung diseases, nausea, respiratory tract diseases, skin allergies and dermatitis. Iron industry toxic chemicals can attack mucous membrane of nose, throat, liver and kidney. They also cause asthma bladder cancer and tumors as per the ESI report concentrated gases from pits are poisonous and cause respiratory tract problems and damage to lung diseases. The study reveals that the following findings which will be very much useful for the abatement methods for the iron industry workers.

REFERENCES

[1]Chatterjee, A., *J. Iron Steel Inst.*, **1995**, *188,* 100-4.

[2]Wilson, A., *Am. Metal Market Energy Spec*., **2001**, *109*, 11.

[3]International Labor Office (ILO).:"*Occupational Safety and Health in the Iron and Steel Industry*", **1983**, International Labor Organization, Geneva.

[4]American Thoracic Society, *Am. Rev. Respiratory Disease*, **1987**, *136*, 1285-98.

[5]Achutan, C. D. and Nemhauser, J., *Health Hazard Evaluation Report*, 2003-0175-3033 COL-FIN Specialty Steel Fallston, Pennsylvania " **2007**, p. 3-9.

[6]Bies, D. A. and Hansen, C. H., *J. Iron Steel Inst.*, **1996**, *190*, 1907-1913.

[7]Diepgen, T. L., Coenrads, P. J., *The epidemiology of occupational contact dermatitis*. In: Kanerva, L., Elsner, P., Wahlberg, J. E., Maibach, H. I., Ed. *Handbook of Occupational Dermatology,* Springer-Verlag, Heidelberg, **2000**, p. 1.

Received: 04.04.2015.
Accepted: 20.07.2015.

SYNTHESIS AND SPECTRAL STUDY OF β-CARBONYLAMINES THROUGH THE USE OF THE MANNICH REACTION

Maged H. Muzael[a]* and Zena Saleh Hassan[a]

Keywords: Mannich reaction, β-carbonylamines, spectral study.

β-Carbonylamines were synthesized using the Mannich reaction. An aldehyde and an amine were condensed to form an imine compound, followed by the addition of concentrated sulphuric acid and acetophenone. The resulting compounds were characterised by IR, ^{1}H and ^{13}C NMR and mass spectroscopy.

*Corresponding Authors
Tel: 009647821092233
E-Mail: alsafee_12@yahoo.com
[a] Department of Chemistry, Thi-Qar University, Thi-Qar, Iraq

Introduction

There exists a definite need for the introduction of new drugs and drug delivery agents with enhanced efficacy and specific targets to counter the rise of multi-drug resistant (MDR) tumours and microbes.[1-5] The Mannich reaction can be a cost and time effective way of converting exsisting drugs into new bioactive molecules, having a greater efficacy than their precursors.[6] It also provides a suitable synthesis method to introduce aminoalkyl substituents into a molecule.[7] In many cases, derivatives from the Mannich reaction exhibit better activity than the analogous parent compound. Moreover, the existences of the Mannich side chain makes the product more soluble and consequently enhances the bioavailability of the drug molecule.[8] Mannich reactions play a vital role in the synthesis of anti-malarial, antitumor, antimicrobial, anti-tubercular, anti-inflammatory and anticonvulsant molecules.[9] The Mannich reaction is the reaction between formaldehyde and an amine to form an imine compound which is followed by adding a ketone-containing acid proton.[10]

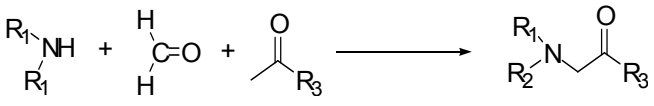

Scheme 1. The preparation of β-carbonyl amines

The Mannich reaction is a very powerful reaction for building carbon-carbon bonds in synthetic organic chemistry. This reaction is particularly useful for the synthesis of β-carbonyl amine derivatives.[11] Due to the significance of the Mannich products in organic synthesis, several variations of this reaction have been developed. The products represent various pharmaceuticals, natural products, and versatile synthetic intermediates.[12] Straight protocols exist for three-component Mannich-type reactions of amines, aldehydes, and ketones in organic solvents. Many attempts have been carried out for the improvement of this type of reaction. Manabe and Kobayashi reported the use of DBSA- to catalyse the three-component Mannich-type reactions in colloidal systems.[1]

The Mannich reaction has many applications in the synthesis of natural products such as peptides, antibiotics and alkaloids.[13-15] The Mannich reaction is particularly useful for the synthesis of β-carbonyl amine derivatives.[11] The reaction is a versatile tool for one pot synthesis.[16,17] The reaction has been useful to synthesise various pharmaceuticals such as anti-malarial, antitumor, antimicrobial, anti-tubercular, anti-inflammatory and anticonvulsant molecules,[9] synthetic intermediates,[12] antibiotics and alkaloids.[13-15] The presence of the side chain on the products increases its solubility that augments the bioavailability of the drug molecules.[8] The reaction is effective to convert existing drugs into new bioactive molecules with greater efficacy than their precursors.[6] Similarly it is a suitable synthesis method to introduce aminoalkyl substituents into a molecule.[7] In many cases the derivatives from the Mannich reaction exhibit better activity than the analogous parent compounds. In this study, the Mannich reaction has been applied to the synthesis of secondary amines.

Experimental

All the chemicals were reagent grade unless stated otherwise and resourced from Sigma and Aldrich. Silica gel (Merck 7736), and silica gel plates for column and thin layer chromatography were Aldrich products, The separated components were detected using variously UV light and I_2. Anhydrous sodium sulfate was used to dry organic solutions. Infrared (IR) spectra were carried out on a Infrared Reflection Absorption Spectroscopy (IRRAS) (4000-400 cm^{-1}) and recorded using Perkin-Elmer tensor 27 as thin film. Melting points were measured using a SMP31melting point apparatus. ^{1}H NMR spectra were carried out on a VARIAN spectrophotometer (300 MHz). The ^{13}C-NMR spectra were recorded, using VARIAN spectrophotometer (75 MHz). HSQC 1H-13C-NMR spectra were recorded, using VARIAN spectrophotometer (600 MHz, 150 MHz).

General Procedure for the preparation of compound 1-3

A) 1,3-Diphenyl-3-(phenylamino)propan-1-one (1).

A mixture of absolute ethanol (40 mL), aniline (5 g, 53.7 mmol, 1 equiv.) and benzaldehyde (5.69 g, 53.7 mmol, 1 equiv) is refluxed for 2 hours in a round-bottomed flask . and monitored by TLC until disappearance of the starting material. The flaski is cooled and a mixture of acetophenone (6.45 g, 53.7 mmol), dissolved in ethanol (10 mL), and concentrated sulphuric acid (1 mL) is added, and this mixture is refluxed at 70 °C for 3 hours. The crude product is filtered and washed with ethanol and recrystallized from ethanol to give a white powder (12.89 gm, yield 87 %), m.p: 145-147 °C; IR: 3385, 3025, 1671, 1600, 1510, 1437, 1417, 1311, 1221 cm^{-1}; ^1H NMR (300 MHz, d_6-DMSO), δ: 7.98-6.2 (15H, m, aromatic), 5.00 (1H, dd, J = 6, 12Hz), 3.64 (1H, dd, J = 9, 18 Hz), 3.34 (1H, s). ^{13}C NMR (75 MHz, d_6-DMSO) δ: 197.28, 147.79, 144.01, 136.77, 134.58, 133.13, 130.62, 130.58, 128.88, 128.78, 128.66, 128.50, 128.27, 128.01, 126.67, 126.61, 122.05, 115.77, 112.80, 52.84, and 46.43. [Found (M+H): Found: 302.1355; required: 302.1364 with existence of dimer at 625.2818.

B) 3-(4-Bromophenylamino)-1,3-diphenylpropan-1-one (2).

A mixture of absolute ethanol (40 mL), 4-bromo aniline (5 g, 53.7 mol) and benzaldehyde (3.1 g, 53.7 mmol, 1 equiv) round-bottomed flask is refluxed for 2 hours and monitored by TLC until disappearance of the starting material. The flask is cooled and a mixture of acetophenone (3.51 g, 53.7 mmol), dissolved in ethanol (10 mL), and concentrated sulphuric acid (1 mL) is added and this reaction mixture is refluxed at 70 °C for 3 hours. The crude product is filtered and washed with ethanol and then recrystallized from ethanol to give a white powder (9.12 g, yield 82 %), 178-177 ° C; IR: 3369, 3019, 1665, 1594, 1577, 1484, 1407, 1303, 1216, 1120 cm^{-1}; ^1H NMR (300 MHz, d_6-DMSO) δ: 7.97-6.45 (14H, m, aromatic), 5.97 (1H, dd, J = 9, 12 Hz), 3.63 (1H, dd, J = 9, 18 Hz), 3.34 (1H, s). ^{13}C NMR (75 MHz, d_6-DMSO) δ: 197.07, 147.07, 143.48, 136.69, 133.11, 131.19, 128.66, 128.34, 138.00, 126.80, 126.57, 114.69, 106.44, 52.76, and 46.31. [Found (M+Na+K): Found: 442.9571; required: 442.3658 with existence of dimer without bromide at 602.2824.

C) 3-(4-Bromophenylamino)-3-(4-chlorophenyl)-1-phenylpropan-1-one (4).

A mixture of absolute ethanol (40 mL), aniline (5 g, 53.7 mol) and 4-chlorobenzaldehyde (4.11 g, 53.7 mmol, 1 equiv) in round-bottomed flask is . refluxed for 2 hours and monitored by TLC until disappearance of the starting material. The flask ic cooled and a mixture of acetophenone (3.51 g, 53.7 mmol) dissolved in ethanol (10 mL) and concentrated sulphuric acid (1 mL) is added to it and this mixture is refluxed at 70 °C for 3 hours. The crude product is filtered and washed with ethanol and then recrystallized from ethanol to give a white powder (10.21 g, yield 84 %), m.p: 92-94 °C; IR: 3390, 1666, 1656, 1592, 1403, 1311, 1217, 1124 $cm^{-1;}$ ^1H NMR (300 MHz, d_6-DMSO) δ: 8.18-6.44 (13H, m, aromatic), 4.98 (1H, dd, J = 9, 20 Hz), 3.63 (1H, dd, J = 9, 18 Hz), 3.35 (1H, s). ^{13}C NMR (75 MHz, d_6-DMSO) δ: 196.83, 189.05, 146.85, 142.55, 142.50, 137.41, 136.60, 135.09, 133.62, 133.21, 131.29, 131.24, 130.57, 128.92, 128.77, 128.57, 128.54, 128.27, 128.00, 122.76, 114.74, 106.68, 52.12, 46.07. [Found (M): 413.0183; required: 413.0182 with existence of dimer without bromide at 671.1816.

Results and Discussion

The Mannich reaction has many applications in the synthesis of natural products and is suitable for the production of secondary amines. [18—23] The preparation of 1,3-diphenyl-3-(phenylamino)propan-1-one is carried out into two steps. The first step of this reaction generates the imine by reacting the aldehyde with the amine. This step is carried under reflux for 1-2 hours whilst monitoring with TLC, Figure 1.[10]

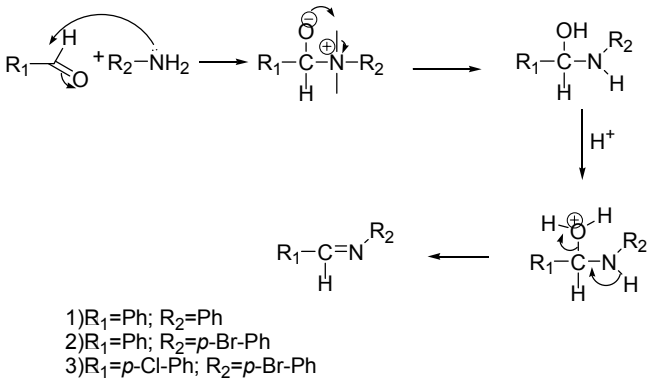

Scheme 2. Formation of imine compounds

The formation of 1,3-diphenyl-3-(phenylamino)propan-1-one is accomplished in the second step by adding acetophenone with concentrated sulphuric acid. The acid attacks the oxygen of the carbonyl group leading to the formation of the enol form and simultaneously, the nitrogen atom of the imine is protonated with formation of ammonium-ion. The equivalent ratio of ketone to amine and aldehyde were 1 equivalent for each one of them.[16-18]

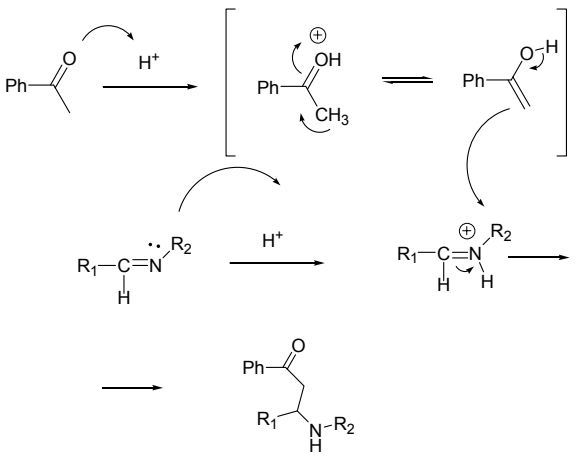

Scheme 3. Suggested mechanism of Mannich reaction using acid as catalyst

IR spectral analysis

All the prepared compounds **1a-1c** showed signals around 3369-3390 cm^{-1} belonging to the NH stretching. The signal which showed at 1665-1671 cm^{-1} belongs to the carbonyl group, while the aromatic C=C showed signals at 1510-1590 cm^{-1}. The C-H aromatic stretching showed absorbance at 3019-3025 cm^{-1}.

^{1}H-NMR analysis

Compound **1a** displayed multiplet signals for the aromatic compound protons between 6.45-7.98 ppm with an integration corresponding to 15 protons. The proton at the chiral centre resonated as a singlet at 3.34 ppm, while the protons of the CH_2 next to the carbonyl showed as a double doublet at 5.00 and 3.64 ppm (Figure 1). Compound **1b** showed a multiplet at 7.97-6.45 ppm for the aromatic protons. The chiral centre proton resonated at 3.34 ppm, while the two protons next to the carbonyl group resonated at 5.97 and 3.63 ppm respectively. Both of the protons showed as doublet of doublets. Compound (**1c**) showed multiplet signals at 8.18-6.44 ppm with an integration of 13 protons for the aromatic protons, while the CH_2 next to the carbonyl resonated at 4.98 and 3.63 ppm respectively. The chiral center proton resonated at 3.35 ppm.

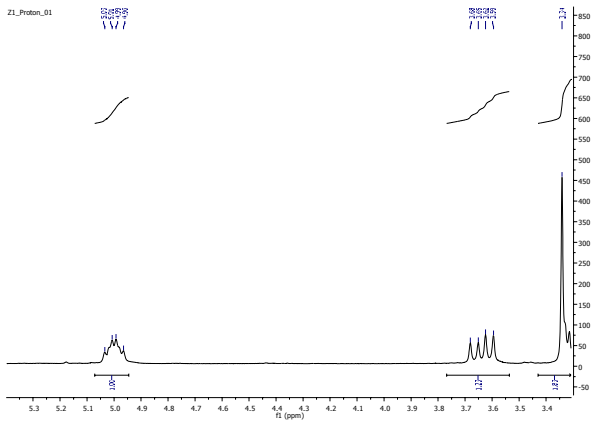

Figure 1. Proton NMR compound 1

^{13}C NMR analysis

Compound **1a** showed the carbonyl carbon signal at 197.28 and the CH_2 and the chiral centre carbon resonated at 46.43, 52.84 respectively. The quaternary carbons showed signals at 147.07, 143.48, 136.69 ppm. The other aromatic carbons resonated between 133 and 106 ppm. Compound **1b** showed a signal at 197.07 ppm for the carbon carbonyl group, while the CH_2 and the chiral center carbon showed 46.31 and 52.76 ppm respectively. The quaternary carbons resonated at 147.07, 143.48 and 136.69 ppm. Compound **1c** showed a signal at 196.83 for the carbon of the carbonyl group, while the CH_2 and the chiral center carbons resonated at 52.12 and 46.07 ppm, respectively. The quaternary carbons resonated at 142.55, 142.50 and 137.41 ppm (Table 1).

Table 1. Comparing between ^{13}C NMR of the prepared compounds

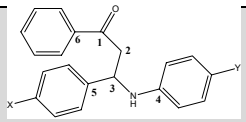

	Compound **1**	Compound **2**	Compound **3**
1	197.28	197.07	196.83
2	46.43	46.31	46.06
3	52.84	52.76	52.12
4	147.79	147.07	146.85
5	144.01	143.48	142.55
6	136.77	136.69	142.50

Mass spectrum analysis

The mass spectrum confirmed the successful preparation of the compounds **1a-1c**. All the prepared compounds showed the ability of forming a dimer Figure 2.

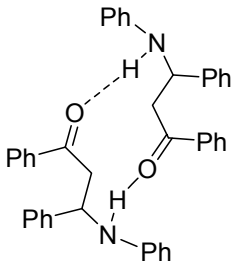

Figure 2. Dimer of the prepared compounds due to hydrogen bonding.

Compound **1a** showed a signal at 324.1355 and another signal at 324.1355. These belong to [M+H], while the signal belonging to the dimer [2M+Na] showed at 625.2818 (Figure 3).

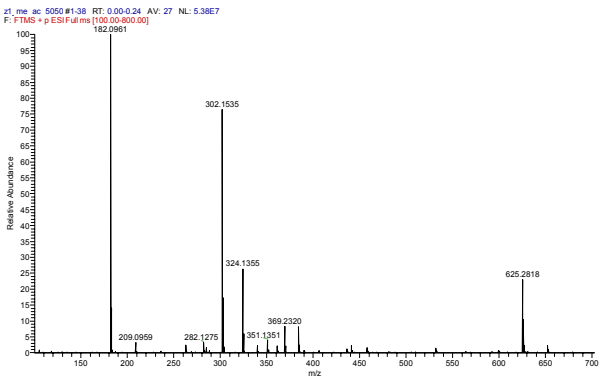

Figure 3. Mass spectra of compound 1a

Compound **1b** showed the existence of bromide since most of signals showed double peaks with gap of 2 Daltons between them. The signal at 380.0634 belongs to [M] while the signal at 442.9571 belongs to M+Na+K, while the signal at 602.2824 belongs to the dimer with the loss of the bromide ions.

The signal at 300.1382 belongs to the [M] without bromide (Figure 4). Compound **1c** showed the molecular ion at 413.0183 and the dimer signal at 671.1816 without bromide (Figure 5).

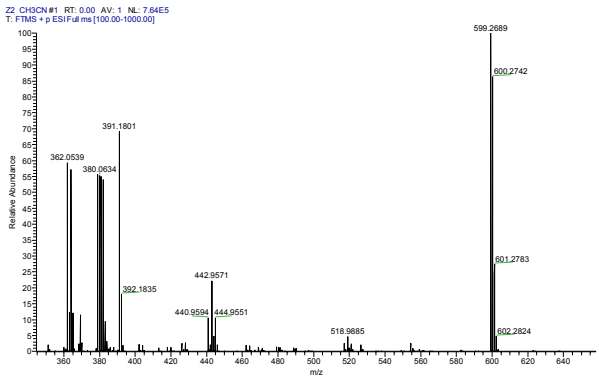

Figure 4. Mass spectra of compound **1b**

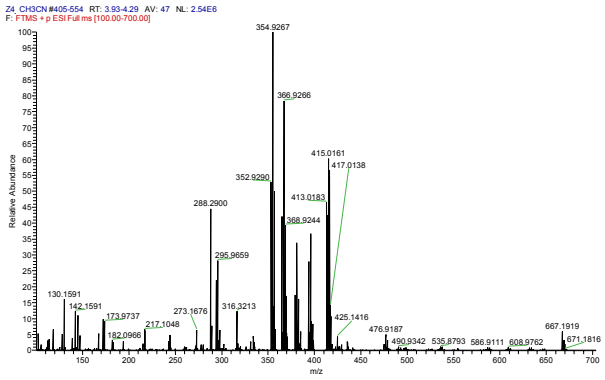

Figure 5. Mass spectra of compound **1b**

References

[1]Kobayashi, S., Ishitani, H., *Chem. Rev.*, **1999**, *99*, 1069.

[2]Kobayashi, S., Mori, Y., Fossey, J. S., Salter, M., M. *Chem. Rev.,* **2011**, *111*, 2626.

[3]Arend, M., Westermann, B., Risch, N., *Angew. Chem., Int. Ed. Engl*.,**1998**, *37*, 1044

[4]Fujisawa, T., Kooriyama, Y., Shimizu, M., *Tetrahedron Lett*., **1996**, *37,* 3881.

[5]Arend, M., Risch, N., *Angew.Chem., Int. Ed. Engl*., **1995**, *34,* 2861.

[6]Kobayashi, S., Ishitani, H., Ueno, M., *J. Am. Chem. Soc.,* **1998**, *120*, 431.

[7]Shioiri, T., Hamada, Y., *Heterocycles*, **1988**, *27*, 1035.

[8]Watson, D. A., Fan, X., Buchwald, S. L., *J. Org. Chem*., **2008**, *73,* 7096.

[9]Rehman, M., Imran, M., Arif, M., Farooq, M., *World Appl. Program.*, **2013**, *3(12)*, 558-564.

[10]Cummings, T., Shelton, J. R., *J. Org. Chem*., **1960**, 25 (3), 419–423.

[11]Shailaja, M., Rao, B., *Indian J. Chem*., **2010**, *49B*, 482.

[12]Guo, Q., Zhao, J., *Org. Lett.*, **2013**, *15*, 508-511

[13]Flávia A. F., da Rosa, Ricardo A., Rebelo, Maria G. Nascimento, *J. Braz. Chem. Soc.,* **2003**, *14*, 11-15.

[14]Gabrielli, S., Ph. D Thesis, UNICAM University, **2010**, P12.

[15]Palomo, C., Oiarbide, M., Landa, A., González-Rego, M., García, J., González, A., Odriozola, J., Martín-Pastor, M., Linden, A., *J. Am. Chem. Soc.,* **2002**, *124*, 8637–8643

[16]Pham, K., Huang, X., Zhang, W., Tetrahedron Lett., **2015,** *56,* 1998–2000

[17]Yang, J. W., Pan, S., List, P., *Org. Synth.*, **2009**, *86*, 11-17

[18]Kobayashi, S., Kiyohara, H., Yamaguchi, M., *J. Am. Chem. Soc*., **2011**, *133*, 708-711.

[19]Xu, L., Xia, C., Li, L., *J. Org. Chem*., **2004**, *69*, 8482-8484.

[20]Josephsohn, N., Snapper, M., Hoveyda,, A., *J. Am. Chem. Soc.,* **2004**, *126*, 3734-3735.

[21]Behbahani, F., Ziarani, L., *Eur. Chem. Bull.*, **2013**, *2(10)*, 782-784

[22]Li Wen Xu, Chun-Gu Xia, Lyi Li., *J. Org. Chem.*, **2004**, *69,* 8482-8484.

[23]List, J., *J. Am. Chem. Soc*., **2000**, *122*, 9336–9337.

Received: 28.05.2015.
Accepted: 21.07.2015.

CRYSTAL STRUCTURE OF (2-METHYLPHENOXY)-ACETOHYDRAZIDE

Naresh Sharma[a]†, P. Naveen[b], Shaukath Ara Khanum[b], Rajni Kant[a] and Vivek K. Gupta[a]*

Keywords: crystal structure, direct methods, hydrogen bond.

The title compound, (2-methyl-phenoxy)-acetohydrazide, was synthesized by refluxing compounds *o*-cresol, ethyl chloroacetate and anhydrous potassium carbonate in the presence of dry acetone. The compound crystallizes in the monoclinic crystal system with space group $P2_1/n$ having unit cell parameters: a = 11.5460(2), b = 6.86700(10), c = 12.7506(3)Å, β = 110.022(2)º and Z = 4 . The crystal structure was solved by direct method using single crystal x-ray diffraction data collected at room temperature and refined by full-matrix least-squares procedures to a final R- value of 0.0377 for 1619 observed reflections. In the crystal structure, molecules are linked into infinite two-dimensional networks by the N–H···N and N–H···O, C−H…O and C−H…π type of hydrogen bonds.

Corresponding Authors*
Mob: +91 9419102467
E-Mail: vivek_gupta2k2@hotmail.com
[a] X-ray Crystallography Laboratory, Post-Graduate Department of Physics & Electronics, University of Jammu, Jammu Tawi -180 006, India. Presently posted at GDC (Boys), Kathua
[b] Department of Chemistry, Yuvaraja's College, University of Mysore, Mysore-570 005, Karnataka, India.

Introduction

Hydrazides have been found to have many commercial and scientific applications.[1-2] It is also used as a raw material in the manufacture of agricultural chemicals, a powerful reducing agent in fuel cells,[3] plant growth regulators in extractive fields[4] and antimicrobial drugs in pharmaceutical applications,[5] precursors for synthesis of heterocycles.[6-7] The vast interest in hydrazine structures is enthused by their value to understand structure–activity relationships and the ongoing search for in vivo active drug lead compound. Careful literature survey for functional groups which could be considered as pharmacophores for the antitubercular activities revealed that the hydrazide moiety is common among most of the antitubercular agents such as salinazid and verazide.[8-9] The structure of the title compound was elucidated by spectral methods and XRD studies.

Experimental

Synthesis

A mixture of *o*-cresol (1.00 g, 0.009 mol), ethyl chloroacetate (1.69 g, 0.01385mol) and anhydrous potassium carbonate (2.86 g, 0.027 mol) was refluxed for 8 hours in the presence of dry acetone. The reaction mixture was cooled and solvent was removed by distillation. The residual mass was diluted with water and extracted with ether. The organic layer was washed with 10 % sodium hydroxide solution, brine and dried over anhydrous sodium sulfate. The solvent was removed under reduced pressure and the resultant liquid was purified by column chromatography to achieve 2-methylphenoxyacetic acid ethyl ester. Finally, (2-methylphenoxy)acetohydrazide as white solid was furnished from stirring 2-methylphenoxy-acetic acid ethyl ester (0.5 g, 0.0025mol) and hydrazine hydrate (0.128 g, 0.0025mol) in the presence of ethanol. The product so obtained was filtered, washed with water and recrystallized from ethanol with 75 % yield, m.p. 128-130 ºC. ^{1}H NMR ($CDCl_3$): 2.2 (s, 3H, CH_3), 4.2 (s, 2H,CH_2) 7.0-7.65 (m, 4H, Ar-H), 9.3 (1H, NH), 4.6 (2H NH_2). IR (Nujol): 1673 (C=O), 3700–3640 cm^{-1} (NH), 3500-3300 cm^{-1} (NH_2). Structure of the title compound is given in Figure 1.

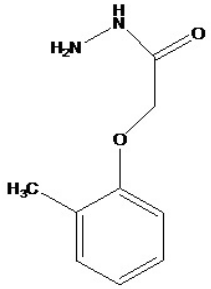

Figure 1. Chemical structure of (2-methylphenoxy)acetohydrazide

X-Ray Structure determination

X-ray intensity data of 46905 reflections (of which 1869 were unique) were collected at 293K on Oxford Diffraction Xcalibur Sapphire3 diffractometer, equipped with graphite-monochromated MoKα radiation (λ=0.71073 Å). The intensities were measured by ω scan mode for θ ranges 3.51 to 26.00° with hkl values $-14 < h < 14$, $-8 < k < 8$, $-15 < l < 15$. 1619 reflections were treated as observed using ($I > 2\sigma(I)$) as criterion. Data were corrected for Lorentz, polarization and absorption factors. The structure was solved by direct methods using SHELXS97.[10] All non-hydrogen atoms of the molecule were located in the best E-

map. Full-matrix least-squares refinement was carried out using SHELXL97.[10] All the hydrogen atoms were geometrically fixed and allowed to ride on their parent C atoms with C-H = 0.93-0.97 Å, and U_{iso}(H) = 1.2-1.5 U_{eq}(C). The final refinement cycles converged to an R = 0.0377 for the observed data. Atomic scattering factors were taken from International Tables for X-ray Crystallography (1992, Vol. C, Tables 4.2.6.8 and 6.1.1.4). The crystallographic data are summarized in Table 1.

Table 1. Crystal data and other experimental details

CCDC Number	**974706**
Crystal description	Block
Crystal size	0.30 x 0.20 x 0.20 mm
Empirical formula	$C_9H_{12}N_2O_2$
Formula weight	180.21
Radiation, Wavelength	MoK_α, 0.71073 Å
Unit cell dimensions	a= 11.5460(2)Å
	b= 6.86700(10) Å
	c= 12.7506(3) Å
	α= 90.0º
	β = 110.022(2)º
	γ= 90.0º
Crystal system, Space group	monoclinic , P2/n
Unit cell volume	949.85(3) Å^3
No. of molecules per unit cell, Z	4
Absorption coefficient	0.091 mm^{-1}
F(000)	384
θ range for entire data collection	3.50 <θ< 29.06
Reflections collected / unique	46905/ 1869
Reflections observed $I > 2\sigma(I)$)	1619
Range of indices	h= -14 to 14
	k=-8 to 8
	l= -51 to 51
No. of parameters refined	131
Final R-factor	0.0377
$w_R(F2)$	0.0955
R_{int}	0.0293
R_σ	0.0477
Goodness-of-fit	1.042
Final residual electron density	-0.164 < Δρ < 0.133 eÅ^{-3}

Results and discussions

There is only one molecule present in an asymmetric unit cell. The bond lengths and bond angles of the title compound are in agreement with the corresponding values obtained in case of related structures.[11] The six C-C bond lengths in the phenyl ring lie in the range 1.366(3)-1.395(2) Å (the average being 1.380(3) Å and the range of these values agree well with the literature value.[12] The C10=O10 distance [1.226(2)Å] confirms the double bond character. The bond angles in the benzene ring vary from 117.6(2) to 121.8(2)º with an average of 119.7(2)º. In the title compound, $C_9H_{12}N_2O_2$, the dihedral angle between the mean planes of the benzene ring (C1–C6) and acetohydrazide group (O10/C10/N11/N12) is 3.1(1)° (Fig. 2). In the molecule, the benzene ring is nearly planar with a maximum deviation of 0.0072 Å observed for the atom C5. In the acetohydrazide group, the N—N bond length is relatively short [1.414(1) Å], suggesting some degree of electronic delocalization in the molecule. An ORTEP[13] view of the title compound with atomic labeling is shown in Fig. 2. The geometry of the molecule was calculated using the PLATON [14] and PARST [15] softwares.

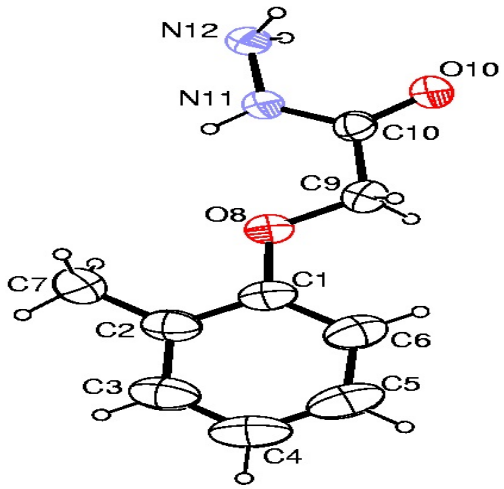

Figure 2. ORTEP view of the molecule of title compound

Table 2. Selected bond lengths (Å) and bond angles (º) for non hydrogen atoms (e.s.d.'s are given in parentheses)

Bond distances(Å)		**Bond angles(°)**	
C(1) - C(2)	1.395(2)	C(2)-C(1)-C(6)	121.3(2)
C(1) - O(8)	1.376(2)	C(6)-C(1)-O(8)	123.6(2)
C(2) - C(7)	1.502(3)	C(1)-C(2)-C(7)	120.8(2)
C(3) - C(4)	1.379(3)	C(3)-C(4)-C(5)	119.6(2)
C(4) - C(5)	1.366(3)	C(1)-O(8)-C(9)	117.4(2)
C(10)-N(11)	1.321(2)	C(9)-C(10)-N(11)	117.7(2)
C(1) - C(6)	1.385(2)	C(2)-C(1)-O(8)	115.1(2)
C(9) - C(10)	1.507(2)	C(1)-C(2)-C(3)	117.6(2)
C(5) - C(6)	1.393(3)	C(3)-C(2)-C(7)	121.5(2)
C(2) - C(3)	1.387(3)	C(2)-C(3)-C(4)	121.8(2)
O(8) - C(9)	1.412(2)	C(4)-C(5)-C(6)	120.7(2)
C(10) -O(10)	1.226(2)	C(1)-C(6)-C(5)	119.0(2)

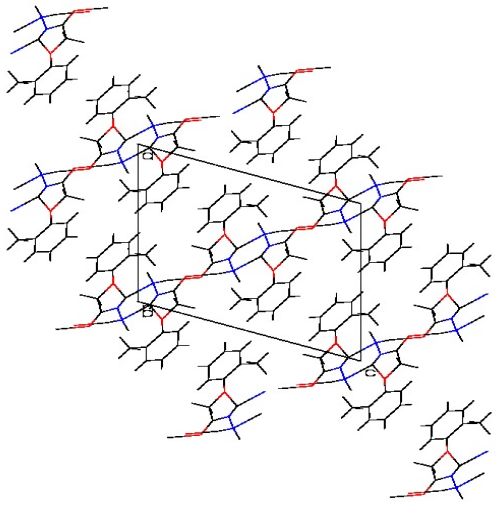

Figure 3. The crystal packing viewed down by the b-axis

Table 3. Geometry of intermolecular hydrogen bonds

D-H…A	D-H (Å)	H…A (Å)	D…A (Å)	θ[D-H…A (°)]
N11−H11…O8	0.86(1)	2.29(1)	2.646(1)	104(1)
C9−H9A...O10^{i}	0.97	2.55	3.277(2)	131.3
N11− H11…N12^{ii}	0.86(1)	2.20(1)	2.918(1)	139(1)
N12− H122…O10^{iii}	0.88(1)	2.06(1)	2.941(1)	170
N12− H121…Cg1^{iv}	0.93(1)	2.58	3.405(1)	147

Symmetry codes: (i) –*x*+1/2, *y*-1/2, -*z*+1/2; (ii) –*x*+1, -*y*+1, -*z*+1; (iii) –*x*+1/2, *y*+1/2, -*z*+1/2; (iv) –*x*+1, -*y*, -*z*+1

A packing view of the molecules in the unit cell viewed down the b-axis is shown in Fig.3. In the crystal structure (Fig. 3), molecules are linked into infinite two-dimensional networks by the N–H···N and N–H···O, C−H…O and C−H…π type of hydrogen bonds. Molecules are packed in layers. The benzene moiety is involved C-H…π contact in the crystal structure. Details of N−H…N, N−H…O, C−H…O and C−H…π interactions are given in Table 2.

Acknowledgments

RK acknowledges the Department of Science & Technology for the single-crystal X-ray diffractometer sanctioned as a National Facility under project No. SR/S2/CMP-47/2003. SAK gratefully acknowledged the financial support provided by the UGC, New Delhi, under the Major research project-scheme [UGC MRP No.F.39-737/2010 (SR) dated 06/01/2010].

References

[1]Rothgery, E. F., *Kirk-Othmer Encyclopedia of Chemical Technology,* 5th ed.; Wiley: Hoboken, NJ, **2005**), *13,* 562.

[2]Schmidt, E. W., *Hydrazine and its Derivatives: Preparation, Properties, Applications*, 2nd ed.; Wiley: Hoboken, NJ, **2001**.

[3]Yamada, K., Yasuda, K., Fujiwara, N., Siroma, Z., Tanaka, H., Miyazaki, Y., and Kobayashi, T., *Electrochem. Commun.*, **2003**, *5*, 892.

[4]Huffman, C. W., Godar, E. M., Ohki, K., Torgeson, D. C., *J. Agric. Food Chem.*, **1968**, *16*, 1041.

[5]Balsamo, A., Macchia, B., Macchia, F., Rossello, A., Giani, R., Pifferi, M. Pinza, G. and Broccali, G., *Chem J. Med.,* **1983**, *26*, 1648.

[6]Hafez, E. A. A., Abed, N. M., Elmoghayer, M. R. H. and El-Agamey, A. G., *Heterocycles*, **1984**, *22*, 1821.

[7]Khanum, S. A., Shashikanth, S., Umesha, S. and Kavitha, R., *Eur. J. Med. Chem.,* **2005**, *40*, 1156.

[8]Bijev, A., *Arzneim.-Forsch/Drug Res.,* **2006**, *56***,** 96e103.

[9]Sbardella, G., Mai, A., Artico, M., Loddo, R., Setzuc, M. G. and Collac, P. L., *Bioorg. Med. Chem. Lett.*, **2004,** *14*, 1537e1541.

[10]Sheldrick, G.M., *Acta Cryst.,* **2008,** *A64*, 112.

[11]Fun, H. K., Quah, C. K., Malladi, S. M. V. A. and Isloor, A. M., *Acta Cryst.***, 2011,** *E67*, o165.

[12]Allen, F. H., Kennard, O., Watson,D. G., Brammer, L., Orpen, A. G., and Taylor, R., *J. Chem.Soc., Perkin Trans-II.*, **1987**, S1.

[13]Farrugia, L. J. *J Appl Cryst.,* **1997,** *30*, 565.

[14]Spek, A. L., *Acta Cryst*., **2009,** *D65*, 148.

[15]Nardelli, M., *J Appl Cryst*., **1995,** *28*, 659.

Received: 04.07.2015.
Accepted: 22.07.2015

CHEMOLYSIS AND EFFECT OF MANDELIC ACID (α-HYDROXYPHENYLACETIC ACID) FOR DISSOLUTION OF URINARY STONE - A STUDY IN VITRO

Ashish Kumar[a]* and Basabi Mahapatra[b]*

Keywords: kidney stone, mandelic acid, nephrolithiasis, ureterolithiasis, cystolithiasis.

A kidney stone, also known as a renal calculus (from the Latin *rēnēs*, "kidneys" and *calculus*, "pebble") is a solid concretion or crystal aggregation formed in the kidneys from dietary minerals in the urine. It was found that mandelic acid is a good inhibitor for calcium carbonate, calcium phosphate and calcium oxalate mineralization and on increasing the strength of inhibitor solution its inhibition efficiency is increased. Mandelic acid is a more efficient inhibitor for calcium carbonate salt comparing to calcium phosphate and calcium oxalate. Simultaneous dynamic model was proved to be more efficient than reservoir dynamic model. Karaunda extract is a good inhibitor for the dissolution of kidney stone. The percentage of dissolution of powder stone is more than the whole renal stone.

*Corresponding Authors
E-Mail: ashpwc2008@rediffmail.com; basabi2011@gmail.com
[a] Department of Chemistry, Patna Women's College, Patna University
[b] Department of Chemistry, Magadh Mahila College, Patna University

INTRODUCTION

Kidney stones are the most common painful urinary disorder. Stones can be treated by various techniques like surgical method or sound therapy method. But these treatments are highly expensive and have not been found so effective in removing the recurrence and also have side effects .It is formed when urine becomes concentrated with certain substances like calcium oxalate, phosphate, carbonate, uric acid and leaves small residues or crystals along the inner surface of the kidney. The urinary stones formation is increasing rapidly in the community and reoccurant stones become a clinical problem. The formation of urinary stones starts in our body when there is pathological disorder in our body & body start excreting excess amount of highly insoluble substances i.e. calcium phosphate , calcium carbonate and calcium oxalate. Stones can be treated by various techniques. But these treatments are highly expensive and these method give only a quick but temporary relief to the patients suffering from renal stone.

Mandelic acid is an aromatic α-hydroxy acid with the molecular formula $C_6H_5CH(OH)COOH$. It is a white crystalline solid that is soluble in water and polar organic solvents. It is a useful precursor to various drugs. Since the molecule is chiral, it exists in either of two enantiomers as well as the racemic mixture, known as paramandelic acid. Its structure is:

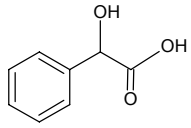

Mandelic acid has a long history of use in the medical community as an antibacterial, particularly in the treatment of urinary tract infections. It has also been used as an oral antibiotic, and as a component of 'chemical face peels', along with other α-hydroxy acids (AHAs).

EXPERIMENTALS

Titration Method

In titration method, we use two models i.e. simultaneous dynamic model (SDM) and reservoir dynamic model (RDM). In the SDM, the two salt forming solutions viz. sodium phosphate and calcium chloride (for calcium phosphate) and the inhibitor (mandelic acid) were taken in three separate burettes (50 ml) and were allowed to fall simultaneously into a 250 ml beaker and continuously stirred on magnetic stirrer (drop wise) with equal speed. At the end the mixture was diluted in a hot water bath for 10 minutes, cooled to room temperature and the precipitate was collected by filtering the solution through a pre-weighed Whatman's filter paper. Next, the filter paper along with the precipitate was dried in an air oven at 80°C, cooled to room temperature and weighed, the weight of the precipitate was determined.In the RDM, the whole amount of inhibitor solution (50 ml) was placed in the beaker in the beginning itself and the two salt forming solutions were allowed to run into it drop wise through burette and the reaction mixture was stirred continuously on a magnetic stirrer.

Table 1. Inhibition of calcium carbonate mineralization by mandelic acid

SALT FORMING SOLUTIONS: 0.01 M $CaCl_2$ and 0.01 M Na_2CO_3					
Inhibitor	**Conc. (M)**	**Wt. of ppt. (in grams)**		**Inhibition Efficiency (%)**	
		SDM	**RDM**	**SDM**	**RDM**
Water	-	0.0105	0.0115	-	-
Mandelic acid	0.1	0.000	0.000	100	100
Mandelic acid	0.01	0.0010	0.0032	90.4	72.7
Mandelic acid	0.001	0.0056	0.0079	41.6	31.3

Table 2. Inhibition of calcium phosphate mineralization by mandelic acid

SALT FORMING SOLUTIONS: 0.01 M $CaCl_2$ and 0.01 M Na_3PO_4					
Inhibitor	**Conc. (M)**	**Wt. of ppt. (in grams)**		**Inhibition efficiency (%)**	
		SDM	**RDM**	**SDM**	**RDM**
Water (blank)	-	0.0432	0.0444	-	-
Mandelic acid	0.1	0.000	0.006	100	98.6
Mandelic acid	0.01	0.0045	0.0136	89.5	69.3
Mandelic acid	0.001	0.0249	0.0321	43.5	27.7

Table 3. Inhibiton of calcium oxalate mineralization by mandelic acid

SALT FORMING SOLUTIONS: 0.01 M $CaCl_2$ and $Na_2C_2O_4$					
Inhibitor	**Conc. (M)**	**Wt. of ppt. (in grams)**		**Inhibition Efficiency (%)**	
		SDM	**RDM**	**SDM**	**RDM**
Water (Blank)	-	0.0482	0.0385	-	-
Mandelic Acid	0.1	0.0205	0.0215	57.4	45.1
MandelicAcid	0.01	0.0273	0.0301	43.1	21.8
MandelicAcid	0.001	0.0364	0.0322	24.4	16.3

Table 4. Dissolution of kidney stone by Karaunda extract

Obs. No.	**Sample**	**Time, h**	**Wt. of stone (in gram)**			**% of dissolution**	**Inhibitor 50 ml**
			Initial	**Final**	**Difference**		
1.	Powder stone	24	0.4254	0.3906	0.0348	8.18%	Karaunda Extract
2.	Powder stone	48	0.3906	0.2650	0.1256	32.1%	
3.	Whole stone	24	0.2007	0.1886	0.0120	6%	
4.	Whole stone	48	0.1886	0.1509	0.03773	20%	

Simultaneous blank experiment with water in place of inhibitor was also carried out for evaluating the inhibitor efficiency of inhibitor compared to water. All experiments were conducted at room temperature (30-34 °C). Percentage efficiency of inhibition (φ) of inhibitor was calculated using the formula:

$$\varphi(\%) = 100\frac{\text{(wt. of ppt. blank set) - (wt. of ppt. in expt. Set)}}{\text{wt. of ppt. in blank set}}$$

DISCUSSION

Study of Tables 1,2,3, indicates that the carbonate and phosphate of this hydroxyacid are good inhibition as compared to oxalate. The inhibition efficiency of carbonate and phosphate of this hydroxyl acid are much more than oxalate of this hydroxyl acid (mandelic acid). Sequestering of these insoluble salts by the mandelic acid might be due to complexation coupled with effective hydrogen – bonding through the -OH groups. Figure 6 indicates that the inhibitory capacity decreases with a decrease in the strength of inhibitor solution. This can be explained as the basis of mass effect. As the concentration of inhibitor decreases the equilibrium might be favouring the precipitation of insoluble salts.

A comparative study of Tables 1, 2 and 3 and Figs. 1, 2 and 3 suggests that the inhibitor is relatively less effective in the inhibition of calcium oxalate mineralization. Comparative studies of different models indicate that the simultaneous dynamic model (SDM) is the most effective one in the inhibition of mineralization. It might be due to

constant stirring, the chelating effect on Ca^{2+} ion with inhibitor and screening effect on precipitation reaction. The whole calculi were treated with 50 ml of Karaunda extract, which contains mandelic acid (50 ml Karaunda juice + 10 ml HCl). The difference in weight of whole calculus, before and after the treatment with it gave a clear indication of dissolution of some ingredients of the calculus, which remained in the solution.

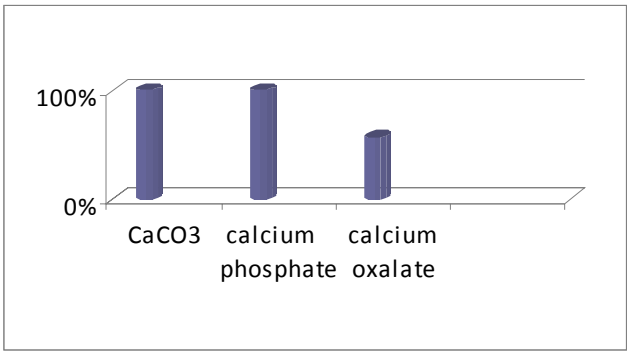

Figure 1. Simultaneous dynamic model. Inhibition efficiency of 0.1 M mandelic acid for mineralization of calcium salts

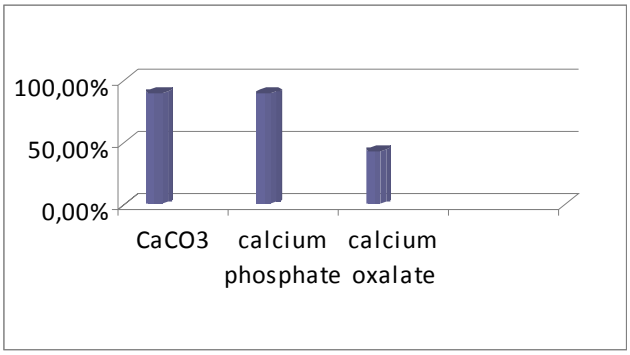

Figure 2. Simultaneous dynamic model. Inhibition efficiency of 0.01 M Mandelic acid for minerlisation of calcium salts

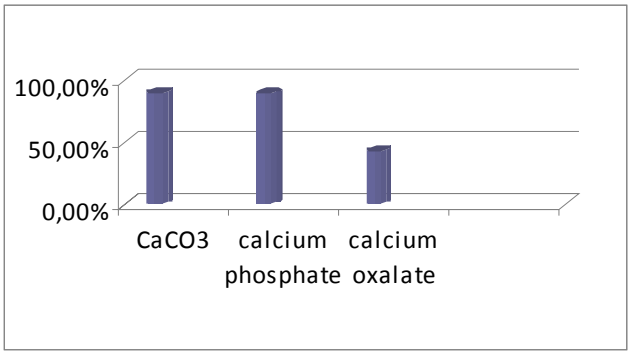

Figure 3. Simultaneous dynamic model. Inhibition efficiency of 0.001 M mandelic acid in minerlisation of calcium salts

The result of our experiment shows that the percentage solubility of the powder renal calculi is 8.1 and 31 % by the Karaunda juice per 24 hours and 48 hours respectively. Our experimental studies have indicated that by increasing the surface area of a calculus available for dissolution of reagents, the % solubility increased. The outer surface of the calculus is much more stubborn & the extract are not able to react so easily to make soluble the ingredient of the calculus. Nevertheless, the dissolution of a part of the ingredient of the whole renal calculus, definitely loosen the hardness of the calculus. This calculus then becomes very much susceptible to attach and the extract then further dissolve the calculus and the calculus crumble.

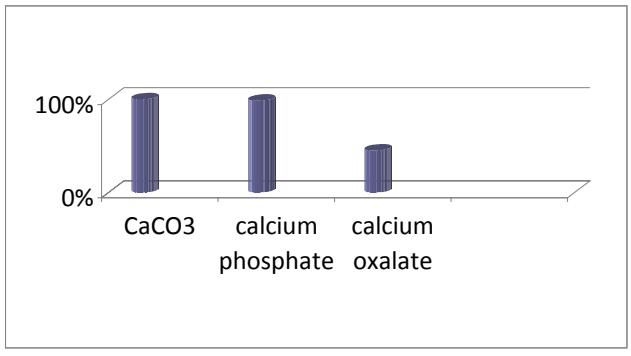

Figure 4. Reservoir dynamic model. Inhibition efficiency of 0.1 M mandelic acid in mineralization of calcium salts

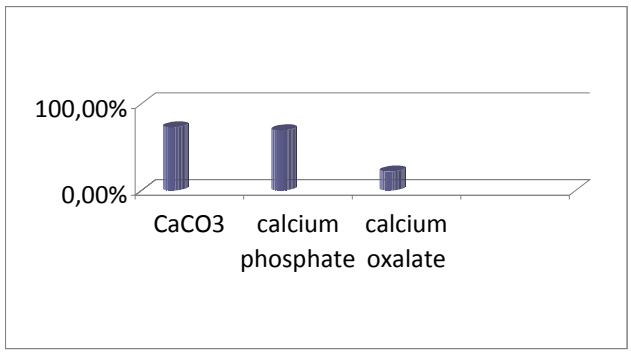

Figure 5. Reservoir dynamic model. Inhibition efficiency of 0.01 M mandelic acid mineralization of calcium salts

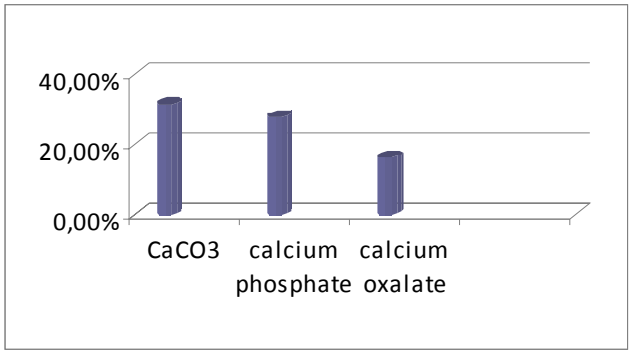

Figure 6. Reservoir dDynamic model. Inhibition efficiency of 0.001 M mandelic acid mineralization of calcium salts

CONCLUSION

The experiments that we performed clearly shows that mandelic acid is a good inhibitor for calcium carbonate, calcium phosphate and calcium oxalate mineralization.

Hence, we conclude that simultaneous dynamic model is more efficient than reservoir dynamic model.

On increasing the strength of inhibitor solution its inhibition efficiency is increased. Inhibitor (mandelic acid) is more efficient for calcium carbonate salt as compare to calcium phosphate and calcium oxalate salt. The inhibition is less effective in the inhibition of calcium oxalate mineralization by SDM with 0.1 M mandelic acid is 57.4 %. With the decrease of the strength of inhibitor the inhibition efficiency of mandelic acid decreases. Karaunda extract is a good inhibitor for the dissolution of kidney stone. The percentage of dissolution of powder stone is more than the whole renal stone.

REFERENCE

[1]Kumar, A., Mahapatra, B., *Acta Cienc. Indica*, **2011**, *37C(4)*, 321.

[2]Kumar, A., Siddiqui, N., Mahapatra, B., *Acta Cienc. Indica,* **2012**, *38C(2)*, 119.

[3]Munoz, J. A., Valiente, M., *Urol. Res*., **2003,** *23(4)*, 267.

[4]Howard, J., Thomas, W. C., Barker, L. N., Smith, L. H., Wadkins, C. L., and Hopkins, J., *Med. J.* **1967**, *120*, 119.

[5]Stamatelou, K. K., Francis, M. E., Jones, C. A., Nyberg, L. M. and Curhan, G. C., *Kidney Int*., **2003**, *63*, 1817.

[6]Smith, L. H., Meyar, J. L. and McCall, J. T., Chemical Nature of Crystal Inhibitors Isolated from Human Urine is Urinary Calculi, *Int. Symp. Renal Stone Res.*, Karge, Basel, **1973,** p. 318.

[7]Parman, M. S., *Br. Med. J.*, **2004**, *328*, 1420.

[8]Seltzer, M. A., Low, R. K., McDonald, M., Shami G. S. and Stolter M. L., *J. Urol.*, **1996**, *1156*, 907.

[9]Selvam, R., Kalaiselvi, P., Govindaraj, A., Murugan, V. B. and Sathish Kumar, A. S., *Pharmacol, Res.*, **2001**, *43*, 89.

Received: 08.03.2015.
Accepted: 23.07.2015.